

Ligand-induced Epitope Masking

DISSOCIATION OF INTEGRIN $\alpha 5 \beta 1$ -FIBRONECTIN COMPLEXES ONLY BY MONOCLONAL ANTIBODIES WITH AN ALLOSTERIC MODE OF ACTION^{*§}

Received for publication, May 6, 2016, and in revised form, July 29, 2016 Published, JBC Papers in Press, August 2, 2016, DOI 10.1074/jbc.M116.736942

A. Paul Mould[‡], Janet A. Askari[§], Adam Byron[¶], Yoshikazu Takada^{||}, Thomas A. Jowitt[‡], and Martin J. Humphries^{§2}

From the [‡]Biomolecular Analysis Core Facility and [§]Wellcome Trust Centre for Cell-Matrix Research, Faculty of Life Sciences, University of Manchester, Manchester M13 9PT, United Kingdom, the [¶]Edinburgh Cancer Research UK Centre, Institute of Genetics and Molecular Medicine, University of Edinburgh, Edinburgh EH4 2XR, Scotland, United Kingdom, and the ^{||}Department of Vascular Biology, VB-1, The Scripps Research Institute, La Jolla, California 92037

We previously demonstrated that Arg-Gly-Asp (RGD)-containing ligand-mimetic inhibitors of integrins are unable to dissociate pre-formed integrin-fibronectin complexes (IFCs). These observations suggested that amino acid residues involved in integrin-fibronectin binding become obscured in the ligand-occupied state. Because the epitopes of some function-blocking anti-integrin monoclonal antibodies (mAbs) lie near the ligand-binding pocket, it follows that the epitopes of these mAbs may become shielded in the ligand-occupied state. Here, we tested whether function-blocking mAbs directed against $\alpha 5 \beta 1$ can interact with the integrin after it forms a complex with an RGD-containing fragment of fibronectin. We showed that the anti- $\alpha 5$ subunit mAbs JBS5, SNAKA52, 16, and P1D6 failed to disrupt IFCs and hence appeared unable to bind to the ligand-occupied state. In contrast, the allosteric anti- $\beta 1$ subunit mAbs 13, 4B4, and AIIB2 could dissociate IFCs and therefore were able to interact with the ligand-bound state. However, another class of function-blocking anti- $\beta 1$ mAbs, exemplified by Lia1/2, could not disrupt IFCs. This second class of mAbs was also distinguished from 13, 4B4, and AIIB2 by their ability to induce homotypic cell aggregation. Although the epitope of Lia1/2 was closely overlapping with those of 13, 4B4, and AIIB2, it appeared to lie closer to the ligand-binding pocket. A new model of the $\alpha 5 \beta 1$ -fibronectin complex supports our hypothesis that the epitopes of mAbs that fail to bind to the ligand-occupied state lie within, or very close to, the integrin-fibronectin interface. Importantly, our findings imply that the efficacy of some therapeutic anti-integrin mAbs could be limited by epitope masking.

Integrins are a large family of α - and β -heterodimeric transmembrane receptors that mediate many cell-cell and cell-matrix interactions (1). These interactions are indispensable for normal development, cell survival, and organ and immune system function. In many disorders, aberrant integrin function plays a role in initiating, maintaining, or exacerbating the disease process. Several integrin family members are important targets for therapy in autoimmunity, thrombosis, fibrosis, and cancer, including $\alpha 4 \beta 1$, $\alpha 4 \beta 7$, $\alpha 11 \beta 3$, $\alpha 5 \beta 1$, $\alpha V \beta 3$, $\alpha V \beta 6$, and $\alpha V \beta 8$ (2, 3). Currently, most efficacious integrin-based therapies involve the use of humanized mAbs that block the ligand-binding site of the integrin (4–6), and these drugs have combined annual sales of over \$2 billion (2). In contrast, some mAb-based therapies have failed in clinical trials (7–9).

Ligand binding to integrins takes place in the so-called “headpiece” domain (10, 11). This region includes the seven-bladed β -propeller domain of the α subunit and the βI and hybrid domains of the β subunit. Loops on the upper surface of the β -propeller and the top face of the βI domain form the ligand-binding pocket (12–17). The metal ion-dependent adhesion site (MIDAS)³ on the top of the βI domain is an essential site for binding to ligands that contain a carboxyl group (such as the RGD peptide sequence) (11, 12, 17, 18). Some integrin ligands contain a second site for integrin binding, such as the Pro-His-Ser-Arg-Asn (PHSRN) synergy sequence in fibronectin (19).

Integrins can exist in different conformational states, and high affinity ligand binding requires an opening of the headpiece (20–22). Headpiece opening involves shifts of the $\alpha 1$ and $\alpha 7$ helices in the βI domain and an outward swing of the hybrid domain away from the β -propeller (11, 23–26). The epitopes of function-blocking anti-integrin α subunit antibodies lie in loops in blades 1–3 of the propeller, overlapping with or close to the loops involved in ligand recognition (27–31). The epitopes of nearly all inhibitory anti- β subunit mAbs lie within the βI domain (11, 21, 32–34). In the integrin $\beta 1$ subunit, these epitopes involve residues in the $\alpha 2$ helix of βI (17, 18, 30), and most of these mAbs appear to block integrin function by preventing an inward movement of the adjacent $\alpha 1$ helix (17, 23).

* This work was supported in part by an award from University of Manchester Intellectual Property Impact Scheme (to A. P. M. and T. A. J.) and Grants 092015 (to M. J. H.) and 105610/Z/14/Z (to M. J. H., A. P. M., and T. A. J.) from the Wellcome Trust. The authors declare that they have no conflicts of interest with the contents of this article.

✂ Author's Choice—Final version free via Creative Commons CC-BY license.

§ This article contains supplemental Video S1.

[‡] Present address: Dept. of Dermatology, Biochemistry and Molecular Medicine, University of California at Davis School of Medicine, Sacramento, California 95817, and the Ph.D. Program for Translational Medicine, College of Medical Science and Technology, Taipei Medical University, Taipei 11031, Taiwan.

² To whom correspondence should be addressed: Faculty of Life Sciences, Michael Smith Bldg., University of Manchester, Oxford Rd., Manchester M13 9PT, United Kingdom. Tel.: 44-161-275-5777; E-mail: martin.humphries@manchester.ac.uk.

³ The abbreviations used are: MIDAS, metal ion-dependent adhesion site; 50K, 50-kDa fragment of fibronectin (3FN6–10); IFC, integrin-fibronectin complex; mu IgG, mouse IgG; RB, running buffer; cRGD, cyclic GCRGDSPCC; SPR, surface plasmon resonance.

Ligand Occupancy Causes Masking of Epitopes in $\alpha 5\beta 1$

Hence, many of these anti- $\beta 1$ mAbs have an allosteric mode of action.

Recently, we showed that RGD-containing ligand-mimetic inhibitors of integrins are unable to dissociate pre-formed IFCs (35), a feature that could have contributed to the failure of compounds such as cilengitide in cancer treatment (36, 37). Our observations provided evidence that the RGD-binding pocket is obscured in the macromolecular ligand-occupied state, *i.e.* integrin residues involved in ligand recognition become buried in the integrin-fibronectin interface. Because the residues that form the epitopes of some function-blocking mAbs lie very close to the ligand-binding pocket, it follows that the epitopes of these mAbs may become obscured in the ligand-occupied state. Hence, these mAbs could fail to bind to, or cause disruption of, IFCs.

Here, we have tested the ability of many different mAbs directed against the α and β subunits of the fibronectin receptor $\alpha 5\beta 1$ to bind to and disrupt IFCs. We show that function-blocking antibodies directed against the $\alpha 5$ subunit fail to dissociate these complexes, suggesting that the epitopes of these mAbs are masked. In contrast, most function-blocking antibodies directed against the $\beta 1$ subunit can disrupt IFCs, demonstrating that the epitopes of these antibodies are still accessible in the ligand-bound state. Additionally, we map the epitope of the unusual anti- $\beta 1$ mAb Lia1/2, which, like the anti- $\alpha 5$ subunit mAbs, fails to dissociate integrin-ligand complexes, and we provide evidence that its epitope partly overlaps with the ligand-binding pocket. Our results suggest that epitopes that are spatially close to residues involved in ligand recognition become obscured in the IFC. An important corollary of these data is that the effectiveness of some therapeutic mAbs could be limited by their epitopes becoming masked in ligand-occupied integrins.

Results

Function-blocking Anti- $\alpha 5$ mAbs Cannot Disrupt Pre-formed $\alpha 5\beta 1$ -Fibronectin Complexes—For surface plasmon resonance (SPR) assays, we used the recombinant proteins $\alpha 5\beta 1$ -Fc (38), the 50-kDa fragment of fibronectin (3FN6–10, “50K”), and a control inactive mutant 50K-KGE in which the RGD sequence is converted to Lys-Gly-Glu (Fig. 1). In this assay (35), 50K is linked to the chip surface, and then recombinant $\alpha 5\beta 1$ -Fc is flowed over the surface for 120 s, leading to the formation of $\alpha 5\beta 1$ -50K complexes. Subsequently, the complexes dissociate slowly (see “Experimental Procedures” for further details). To test the ability of mAbs to affect the stability of IFCs, mAbs were injected during the dissociation phase as described previously (*i.e.* post-integrin injection) (35). Three possible outcomes would be anticipated as follows: (i) if mAbs were unable to bind to the complexes, there would be no effect on the dissociation rate; (ii) if mAbs could bind to and cause disruption of IFCs, there would be an observed increase in the dissociation rate; or (iii) if mAbs could bind to IFCs without causing disruption, there would be an increase in SPR signal due to mAb binding.

First, we tested whether the function-blocking anti- $\alpha 5$ subunit mAbs JBS5, SNAKA52, 16, and P1D6 were able to alter the dissociation rate of integrin-50K complexes. Key epitope residues of these mAbs lie in loop regions of the β -propeller

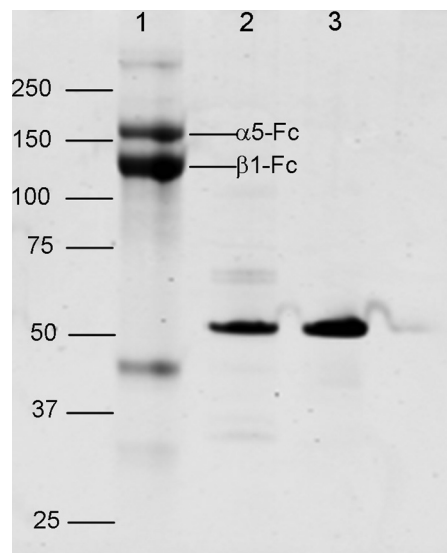


FIGURE 1. SDS-PAGE of the recombinant integrin and fibronectin fragments used in these experiments. Samples were run on a 4–12% gel under reducing conditions. Lane 1, $\alpha 5\beta 1$ -Fc; lane 2, biotinylated 50K; lane 3, biotinylated 50K-KGE. Positions of molecular mass markers (kDa) are shown. A band in the $\alpha 5\beta 1$ -Fc sample running just below the 50-kDa marker probably corresponds to a partial cleavage product of the $\alpha 5$ light chain-Fc subunit ($\alpha 5$ -Fc).

domain (Table 1). The results (Fig. 2, *cyan sensorgrams*) showed that none of these mAbs caused an increase in the dissociation rate relative to the buffer-only channel (Fig. 2, *red sensorgrams*). As a control, when these mAbs were added to the integrin before binding to the fibronectin fragment (*i.e.* pre-integrin injection), almost complete inhibition of complex formation was observed (Fig. 2, *blue sensorgrams*). Hence, although these mAbs could prevent complexes from forming, they could not disrupt pre-formed IFCs, suggesting that these mAbs are unable to bind to the complexes.

Function-blocking Anti- $\beta 1$ mAbs, with the Exception of Lia1/2, Can Disrupt Pre-formed $\alpha 5\beta 1$ -Fibronectin Complexes—Next, we tested whether the function-blocking anti- $\beta 1$ subunit mAbs 13, 4B4, AIIB2, and Lia1/2 were able to increase the dissociation rate of IFCs. Key epitope residues of the mAbs 13, 4B4, and AIIB2 lie in the $\alpha 2$ helix region of the $\beta 1$ domain (Table 1), but the exact Lia1/2 epitope location is unknown. The results (Fig. 3, *cyan sensorgrams*) showed that 13, 4B4, and AIIB2 caused a marked (~ 4 -fold) increase in the dissociation rate, whereas Lia1/2 did not affect the dissociation rate (Fig. 3 legend). When these mAbs were pre-mixed with the integrin before binding to the fibronectin fragment (Fig. 3, *blue sensorgrams*), 13, 4B4, and AIIB2 showed a partial ($\sim 70\%$) inhibition of complex formation, whereas Lia1/2 caused a near-complete inhibition, comparable with that seen for the function-blocking anti- $\alpha 5$ mAbs. Hence, 13, 4B4, and AIIB2 can bind to and disrupt IFCs; members of this group of mAbs appear to have an allosteric mode of action (35). In contrast, Lia1/2 cannot bind to or disrupt IFCs and seem to have properties similar to the anti- $\alpha 5$ mAbs.

Non-function-blocking mAbs Can Bind to but Do Not Disrupt Pre-formed $\alpha 5\beta 1$ -Fibronectin Complexes—Finally, we tested the effect of the non-function-blocking anti- $\alpha 5$ subunit (Fig. 4,

TABLE 1

The properties and epitope location of anti- $\alpha 5$ and anti- $\beta 1$ mAbs used in this study

mAb	Property	Epitope location
JBS5	Function blocking	$\alpha 5$ β -propeller domain Ser-85 (27) ¹
SNAKA52	Function blocking	$\alpha 5$ β -propeller domain Ser-85 (27) ¹
P1D6	Function blocking	$\alpha 5$ β -propeller domain Leu212 (27)
16	Function blocking	$\alpha 5$ β -propeller domain Glu-126/Leu-128/Trp-157 (27, 68, 69) ^a
VC5	Neutral	$\alpha 5$ β -propeller domain (70)
11	Neutral	$\alpha 5$ Calf-2 domain His-770/Arg-772 (71)
SNAKA51	Activating (weak)	$\alpha 5$ Calf-1/Calf-2 domains (39, 68)
13	Function blocking	$\beta 1$ $\beta 1$ domain Asn-207–Lys-218 (32)
4B4	Function blocking	$\beta 1$ $\beta 1$ domain Ly-s218 (32)
A1IB2	Function blocking	$\beta 1$ $\beta 1$ domain Val-211 (32)
Lia1/2	Function blocking	$\beta 1$ unknown
3S3	Function blocking	$\beta 1$ unknown
6S6	Function blocking	$\beta 1$ unknown
HUTS-4	Activating (weak)	$\beta 1$ hybrid domain Ser-370/Glu-371/Lys-417 (24)
JB1A	Neutral	$\beta 1$ hybrid domain Asn-82–Lys-87 (72)
8E3	Activating (weak)	$\beta 1$ PSI domain Glu-4 (40)
TS2/16	Activating (strong)	$\beta 1$ $\beta 1$ domain Asn-207–Lys-218 (32)
K20	Neutral	$\beta 1$ I-EGF domains (32)

^a In the original paper (27), Ser-85 was incorrectly designated as Ser-75, and Glu-126 and Leu-128 were incorrectly designated as Glu-116 and Leu-118.

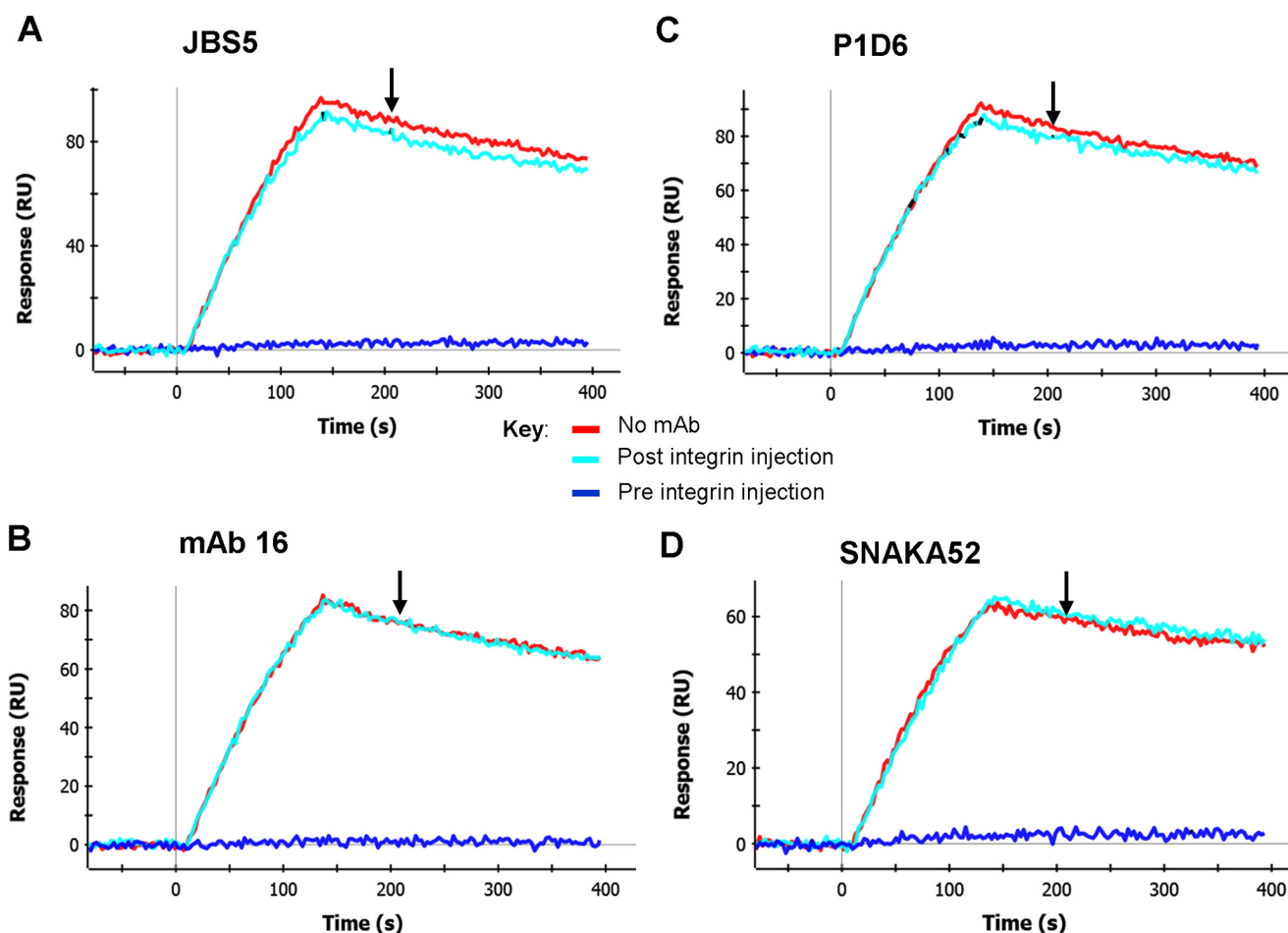


FIGURE 2. Effect of function-blocking anti- $\alpha 5$ mAbs on integrin-fibronectin complexes. A–D, binding of $\alpha 5 \beta 1$ -Fc to 50K fibronectin fragment took place for 120 s in three parallel channels in RB. In the blue sensorgrams, integrin was pre-mixed with 100 nM of the indicated anti- $\alpha 5$ mAb. 60 s after the start of the dissociation phase, at the time indicated by the downward-pointing arrow (~ 207 s), either RB alone (red and blue sensorgrams) or RB with 100 nM mAb (cyan sensorgrams) was injected for 120 s. A, dissociation rate in buffer alone was $9.73 \times 10^{-4} \text{ s}^{-1}$ and in the presence of JBS5 was $8.98 \times 10^{-4} \text{ s}^{-1}$. B, dissociation rate in buffer alone was $9.75 \times 10^{-4} \text{ s}^{-1}$ and in the presence of mAb was $16.987 \times 10^{-4} \text{ s}^{-1}$. C, dissociation rate in buffer alone was $9.70 \times 10^{-4} \text{ s}^{-1}$ and in the presence of P1D6 was $9.24 \times 10^{-4} \text{ s}^{-1}$. D, dissociation rate in buffer alone was $7.93 \times 10^{-4} \text{ s}^{-1}$ and in the presence of SNAKA52 $6.44 \times 10^{-4} \text{ s}^{-1}$. Dissociation rates were measured between 208 and 330 s. Similar results were obtained in three separate experiments.

A–C) and anti- $\beta 1$ subunit (Fig. 4, D–F) mAbs on $\alpha 5 \beta 1$ -fibronectin complexes. The epitopes of these mAbs lie outside the ligand-binding region (Table 1). All of the mAbs caused an increase in SPR signal when added during the dissociation

phase, indicative of mAb binding to the complexes (Fig. 4, cyan sensorgrams) without causing disruption. With the exception of JB1A, none of these antibodies caused an increase in the dissociation rate of the complexes subsequent to mAb binding (Fig. 4

Ligand Occupancy Causes Masking of Epitopes in $\alpha 5\beta 1$

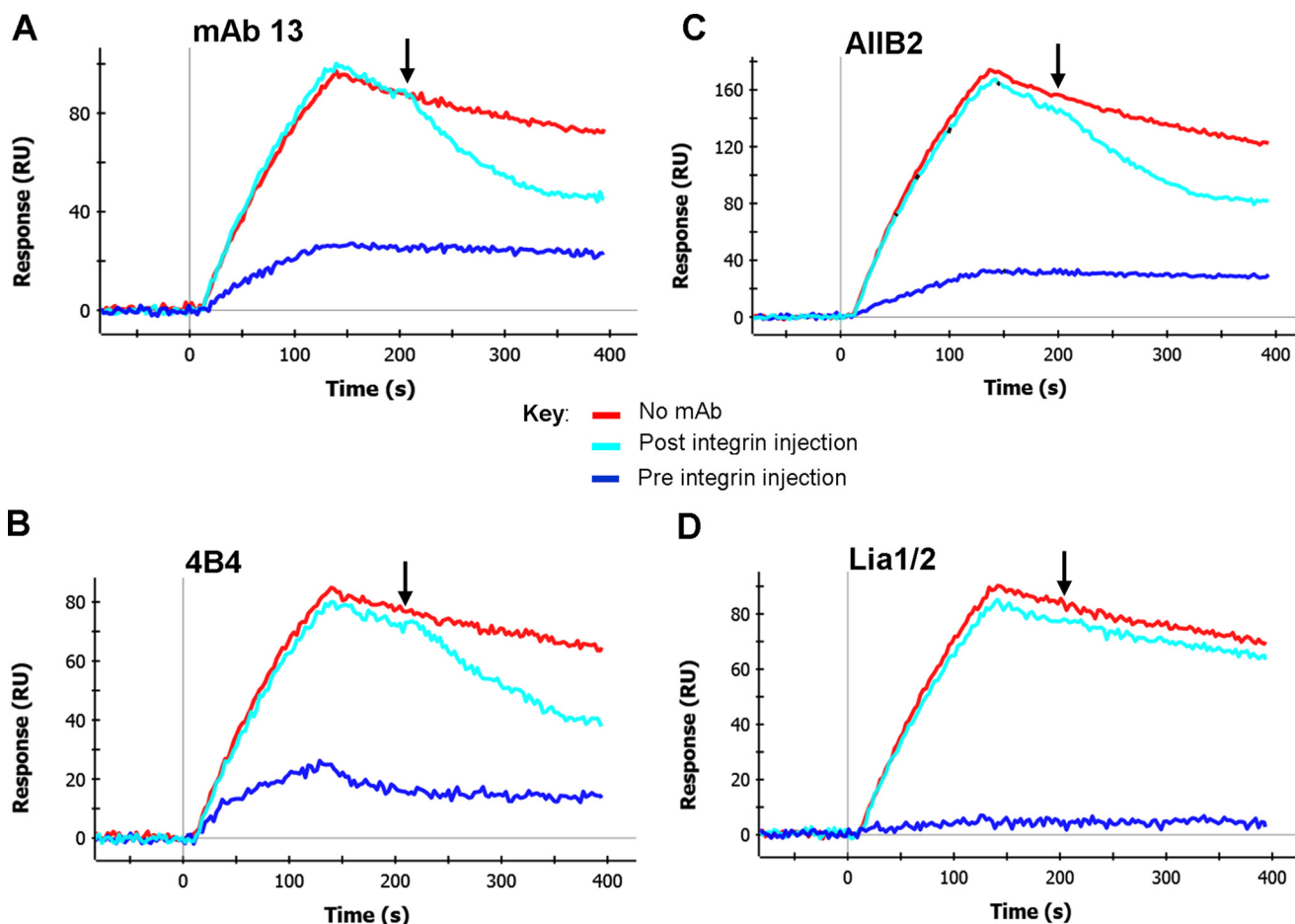


FIGURE 3. Effect of function-blocking anti- $\beta 1$ mAbs on integrin-fibronectin complexes. A–D, binding of $\alpha 5\beta 1$ -Fc to 50K fibronectin fragment took place for 120 s in three parallel channels in RB. In the *blue sensorgrams*, integrin was pre-mixed with 100 nM of the indicated anti- $\beta 1$ mAb. 60 s after the start of the dissociation phase, at the time indicated by the *downward-pointing arrow* (~ 207 s), either RB alone (*red and blue sensorgrams*) or RB with 100 nM mAb (*cyan sensorgrams*) was injected for 120 s. Dissociation rates were measured during the buffer or mAb injection step (208–228 s). A, dissociation rate in buffer alone was $1.11 \times 10^{-3} \text{ s}^{-1}$ and in the presence of mAb 13 was $4.98 \times 10^{-3} \text{ s}^{-1}$. B, dissociation rate in buffer alone was $1.01 \times 10^{-3} \text{ s}^{-1}$ and in the presence of 4B4 was $4.04 \times 10^{-3} \text{ s}^{-1}$. C, dissociation rate in buffer alone was $1.37 \times 10^{-3} \text{ s}^{-1}$ and in the presence of AIIB2 was $4.31 \times 10^{-3} \text{ s}^{-1}$. D, dissociation rate in buffer alone was $0.91 \times 10^{-3} \text{ s}^{-1}$ and in the presence of Lia1/2 was $1.05 \times 10^{-3} \text{ s}^{-1}$. Similar results were obtained in three separate experiments.

legend). Furthermore, all of the other non-function-blocking mAbs were able to slightly decrease the dissociation rate, even though the measured dissociation rates of mAb- $\alpha 5\beta 1$ -fibronectin complexes will also include a component from the dissociation of mAb binding to the integrin. Some of these mAbs (SNAKA51, 8E3, and HUTS-4) have previously been shown to be weakly activating and hence may be capable of directly stabilizing IFCs (24, 39, 40). All the mAbs showed no inhibition of complex formation when pre-mixed with the integrin (data not shown). In summary, although all these non-function-blocking mAbs bound to IFCs, no disruption of the complexes was observed.

Lia1/2 Binding to $\alpha 5\beta 1$ Is Strongly Perturbed by Ligand Recognition—The unusual properties of Lia1/2 prompted us to explore further its mechanism of action. We previously showed that the binding of some function-blocking mAbs to $\beta 1$ is inhibited by RGD-containing peptides and fibronectin fragments (15, 41). We therefore tested the effect of 50K and cRGD on the binding of Lia1/2 to $\alpha 5\beta 1$, and we simultaneously compared the effect of these reagents on the binding of mAbs 13 and 4B4. The results (Fig. 5, A and B) showed that Lia1/2 binding was more strongly inhibited by 50K and cRGD than was the

binding of mAbs 13 and 4B4. In control experiments (data not shown), the 50K-KGE mutant protein had no effect on mAb binding. We next tested whether the cRGD peptide acted as an allosteric or a competitive inhibitor of Lia1/2 binding (Fig. 5C). In this experiment, the effect of cRGD on binding of Lia1/2 to $\alpha 5\beta 1$ was tested over a 10-fold range of mAb concentrations. The results (Fig. 5 legend) showed that the concentration of cRGD peptide for half-maximal inhibition increased at the higher antibody concentration. If ligand behaved as a purely allosteric inhibitor of mAb binding, the concentration of peptide for half-maximal inhibition should be unchanged, and the maximal extent of inhibition should decrease with increased antibody concentration (as we previously observed for mAb13 binding (41)). In contrast, if ligand behaved as a direct competitive inhibitor of mAb binding, the concentration of ligand for half-maximal inhibition should increase in proportion to the antibody concentration, and the maximal extent of inhibition should be unchanged. However, for Lia1/2 binding, we observed that the concentration of cRGD peptide for half-maximal inhibition increased 2–3-fold for a 10-fold increase in antibody concentration, and the maximal extent of inhibition decreased.

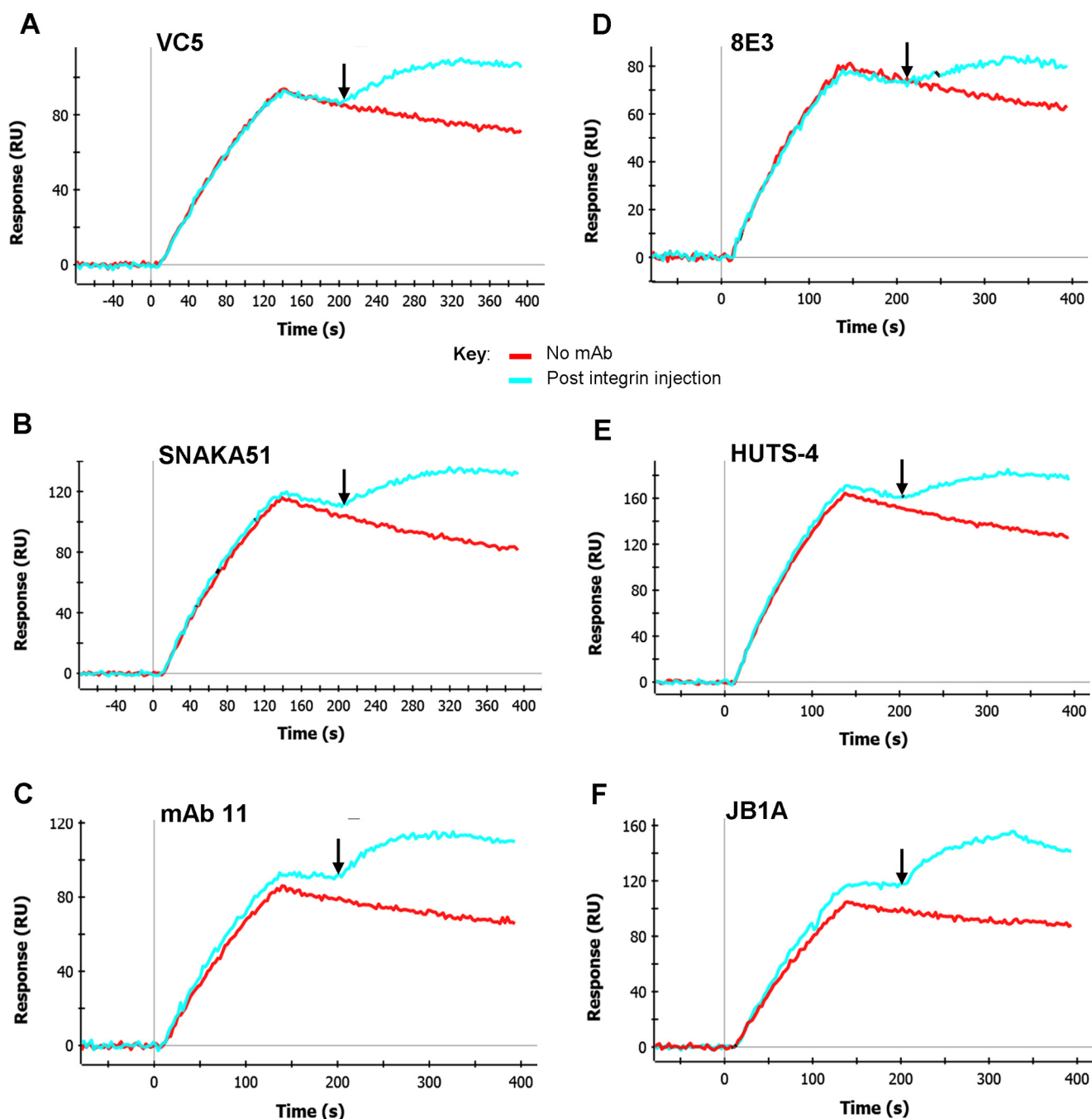


FIGURE 4. **Effect of non-function-blocking anti- $\alpha 5$ and anti- $\beta 1$ mAbs on integrin-fibronectin complexes.** A–F, binding of $\alpha 5\beta 1$ -Fc to 50K fibronectin fragment took place for 120 s in three parallel channels in RB. In the *blue* sensorgrams, integrin was pre-mixed with 100 nM of the indicated anti- $\alpha 5$ mAb (A–C) or anti- $\beta 1$ mAb (D–F). 60 s after the start of the dissociation phase, at the time indicated by the *downward-pointing arrow* (~207 s), either RB alone (*red* and *blue* sensorgrams) or RB with 100 nM mAb (*cyan* sensorgrams) was injected for 120 s. Dissociation rates were measured after the end of the buffer or mAb inject step (330–390 s) for $\alpha 5\beta 1$ -fibronectin complexes (*red* sensorgrams) or mAb- $\alpha 5\beta 1$ -fibronectin complexes (*cyan* sensorgrams). A, dissociation rates were 8.75×10^{-4} and $3.59 \times 10^{-4} \text{ s}^{-1}$, respectively. B, dissociation rates were 11.3×10^{-4} and $3.26 \times 10^{-4} \text{ s}^{-1}$, respectively. C, dissociation rates were 8.47×10^{-4} and $4.47 \times 10^{-4} \text{ s}^{-1}$, respectively. D, dissociation rates were 7.55×10^{-4} and $4.33 \times 10^{-4} \text{ s}^{-1}$, respectively. E, dissociation rates were 8.10×10^{-4} and $3.28 \times 10^{-4} \text{ s}^{-1}$, respectively. F, dissociation rates were 6.73×10^{-4} and $12.9 \times 10^{-4} \text{ s}^{-1}$, respectively. Similar results were obtained in three separate experiments.

These data indicate that the inhibition by cRGD is partly competitive and partly allosteric in nature.

Epitope Mapping of Lia1/2—The epitope of Lia1/2 has not been accurately mapped. We initially used mouse/human and chicken/human $\beta 1$ chimeras to localize the epitope to a specific region of $\beta 1$. The results (Table 2) showed that the Lia1/2 epitope was included in a region containing amino acids 190–304, which is part of the $\beta 1$ domain. The same region has pre-

viously been shown to include the epitopes of mAbs 13, 4B4, AIB2, and TS2/16 (32). Because there are only five amino acid changes in this region from mouse to human $\beta 1$, point mutations in each of these five residues (Asn-207, Lys-208, Val-211, Lys-218, and Met-287) were made, essentially as described previously (32). The results (Tables 3 and 4) showed that no single point mutation abrogated Lia1/2 binding, although this is also the case with several other mAbs that bind to this region,

Ligand Occupancy Causes Masking of Epitopes in $\alpha 5\beta 1$

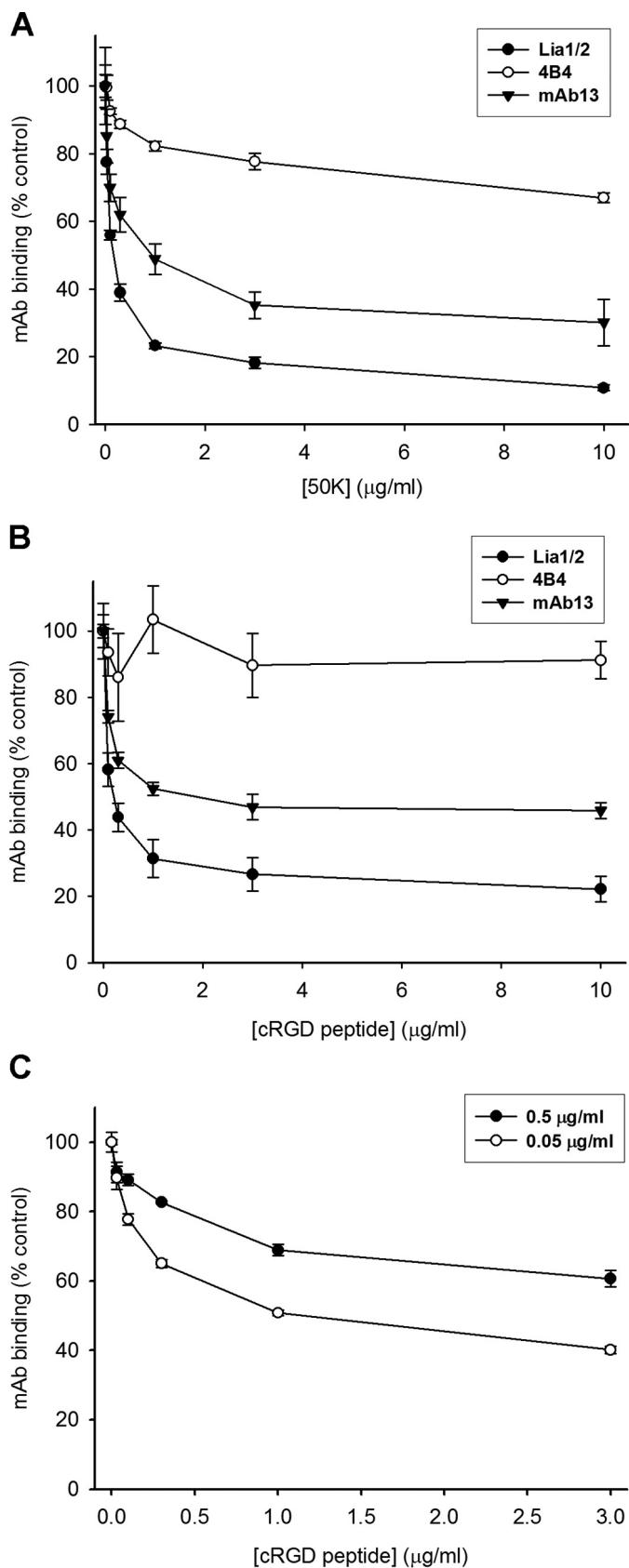


FIGURE 5. Effect of 50K fibronectin fragment and cyclic RGD peptide on Lia1/2 binding to $\alpha 5\beta 1$. A and B, ability of 50K (A) or cyclic RGD peptide (B) to inhibit binding of Lia1/2 (closed circles) to $\alpha 5\beta 1$ was tested in a solid-phase assay, in parallel with mAbs 13 (closed triangles) and 4B4 (open circles). C, test of competitive inhibition by cRGD peptide on Lia1/2 binding to $\alpha 5\beta 1$. The

including 13 and TS2/16 (32). Four of the mutated residues, Asn-207, Lys-208, Val-211, and Lys-218, lie within the $\alpha 2$ helix region of the $\beta 1$ domain (17, 18). However, Lia1/2 did react with the previously described “CH mutant” (32), which contains the sequence of human $\beta 1$ residues 207–218 in the context of chicken $\beta 1$ (data not shown), and hence its epitope directly overlaps with that of other function-perturbing anti- $\beta 1$ mAbs.

Anti- $\beta 1$ mAbs That Induce Homotypic Aggregation Fail to Disrupt $\alpha 5\beta 1$ -Fibronectin Complexes—Treatment of mononuclear cells with some function-blocking anti- $\beta 1$ mAbs can cause homotypic cell aggregation (42–47), a poorly understood phenomenon that requires integrin-mediated intracellular signaling (42, 48). The epitopes of many function-blocking anti- $\beta 1$ mAbs have previously been sub-divided into two sub-classes, A1 and A2; although the epitopes of these two classes overlap, members of the A1 class can be distinguished from those of the A2 class by their ability to induce homotypic aggregation (44). The A1 class is known to include Lia1/2 (44). We tested the ability of the function-blocking anti- $\beta 1$ mAbs used in this study to induce homotypic aggregation of Jurkat T-lymphoblastic cells, using the activating mAb TS2/16 as a negative control (Fig. 6, A–F). Our results showed that mAb 13 did not cause cell aggregation, and 4B4 and AIIB2 caused only the appearance of some small aggregates of cells. In contrast, Lia1/2 caused the appearance of very large clusters of cells, and so was the only mAb of this group able to strongly trigger homotypic aggregation. Hence, mAbs 13, 4B4, and AIIB2 are members of the A2 class.

We next tested whether other anti- $\beta 1$ mAbs that have been reported to induce homotypic aggregation had properties similar to those of Lia1/2. We obtained the mAbs 3S3 and 6S6 (47) and confirmed that these mAbs were able to strongly induce cell aggregation (Fig. 6, G and H). It has been previously shown that cell aggregation induced by some anti- $\beta 1$ mAbs can be specifically inhibited by ceramide analogs (42). Aggregation caused by Lia1/2, 3S3, and 6S6 was blocked to a similar extent by the cell-permeable compound *N*-hexanoyl-*D*-sphingosine (C_6 -ceramide) (Fig. 7), indicating that all three mAbs trigger cell aggregation via a common mechanism involving intracellular signaling.

We then examined the effect of 3S3 and 6S6 on the formation and dissociation of $\alpha 5\beta 1$ -fibronectin complexes (Fig. 8, A and B). The two mAbs inhibited the formation of IFCs (Fig. 8, A and B, blue sensorgrams), although they were less potent inhibitors of complex formation than Lia1/2. Significantly, like Lia1/2, both 3S3 and 6S6 were unable to disrupt pre-formed IFCs (Fig. 8, A and B, cyan sensorgrams). A very small increase in signal was consistently observed during the time window that these mAbs were injected over the complexes, suggesting that they could bind very weakly to the complexes, although this binding had no effect on the overall dissociation rate.

effect of cRGD was tested at 10-fold different concentrations of Lia1/2 (0.05 and 0.5 $\mu\text{g/ml}$; open and closed circles, respectively). In this experiment, the concentration of cRGD for half-maximal inhibition of Lia1/2 binding was estimated by non-linear regression analysis to be 0.231 and 0.503 $\mu\text{g/ml}$ for 0.05 and 0.5 $\mu\text{g/ml}$ of Lia1/2, respectively. In $n = 4$ experiments, the concentrations of cRGD for half-maximal inhibition were 0.211 ± 0.059 and 0.538 ± 0.130 $\mu\text{g/ml}$ for 0.05 and 0.5 $\mu\text{g/ml}$ of Lia1/2, respectively (mean \pm S.D., $p < 0.005$, Student's *t* test).

TABLE 2**The reactivity of Lia1/2 to wild-type and different chimeric $\beta 1$ chains by flow cytometry**

The numbers in the table represent mean fluorescence intensity values in the typical experiments using CHO cells stably expressing wild-type or chimeric $\beta 1$. /+ represents positive reactivity of the transfected cells to the mAbs; /- represents no reactivity. Mouse IgG was used as a control.

Antibody	CHO	h587/m	h425/m	h354/m	h304/c	h189/c
Mouse IgG	3.52	4.48	4.05	4.92	6.24	5.49
Lia1/2	4.33/-	75.01/+	40.26/+	163.51/+	71.45/+	5.22/-

TABLE 3**Reactivity of Lia1/2 to wild-type and mutant human $\beta 1$ chains by flow cytometry**

Human $\beta 1$ chains with human-to-mouse mutations were transiently expressed on CHO cells, and the reactivity of the cells to mAbs was examined by flow cytometry; numbers represent mean fluorescence intensity values. Clonal CHO cells stably expressing human wild-type $\beta 1$ were used as positive control. /+ represents positive reactivity to the mAbs.

Antibody	CHO	N207D	K208R	V211F	K218Q	Human $\beta 1$
Mouse IgG	3.93	2.73	4.47	2.99	5.08	3.92
Lia1/2	4.61/-	183.79/+	126.30/+	108.92/+	54.86/+	260.94/+

TABLE 4**Reactivity of Lia1/2 to wild-type and mutant human $\beta 1$ chains by flow cytometry**

CHO-K1 cells transiently expressing wild-type or M287V mutant $\beta 1$ -GFP were examined by flow cytometry for reactivity with TS2/16 or Lia1/2; numbers represent MFI values. /+ represents positive reactivity to the mAbs. Mouse IgG was used as a control.

Antibody	M287V	Human $\beta 1$
Mouse IgG	247	270
TS2/16	11,512/+	11,780/+
Lia1/2	14,856/+	14,111/+

The epitopes of 3S3 and 6S6 have not been localized to a specific region of $\beta 1$. To test whether the epitopes of these mAbs map to the same region of $\beta 1$ as Lia1/2, we used a competitive ELISA (Fig. 8C). In this assay, we used biotinylated Lia1/2 and competed its binding to $\alpha 5\beta 1$ using a large excess of unlabeled mAbs. The binding of biotinylated Lia1/2 was abrogated by the mAbs 13, 4B4, and AIIB2, as well as TS2/16 (32), in agreement with our epitope mapping data above. Significantly, both 3S3 and 6S6 also strongly inhibited Lia1/2 binding, whereas the control mAbs 8E3 and K20, whose epitopes lie outside of the $\beta 1$ domain (Table 1), had little effect on Lia1/2 binding. Therefore, the epitopes of 3S3 and 6S6 appear to be closely overlapping with the epitope of Lia1/2. Hence, like Lia1/2, 3S3 and 6S6 are members of the A1 class.

New Model of the $\alpha 5\beta 1$ -Fibronectin Complex Supports the Epitope-masking Hypothesis—The failure of some function-blocking mAbs to disrupt IFCs suggests that these mAbs are unable to bind to IFCs because their epitopes become masked in the ligand-bound state of $\alpha 5\beta 1$. To test this possibility further, a model of the $\alpha 5\beta 1$ -fibronectin complex (Fig. 9 and supplemental Video S1) was constructed based on the crystal structure of 3FN10 bound to $\alpha V\beta 3$ (49) and the NMR structure of murine 3FN9,10 (50). 3FN9 contains the synergy region, whereas 3FN10 contains the RGD sequence. The orientation of 3FN9,10 was guided by docking the fragment onto the $\alpha 5\beta 1$ crystal structure (18), with 3FN10 in the same orientation as in the $\alpha V\beta 3$ crystal structure (49). Only minimal adjustments in the position of 3FN9 were required to prevent steric clashes between 3FN9 and β -propeller residues (see “Experimental Procedures”). To estimate the antibody-accessible surface, we rolled a 20-Å sphere (the approximate size of a Fab fragment) over the structure (51). The results (Fig. 10) indicated that $\alpha 5$

residues Leu-212 (P1D6 epitope), Glu-126/Leu-128/Trp-157 (mAb 16 epitope), and Ser-85 (JBS5 and SNAKA52 epitopes) would not be accessible in the ligand-occupied state. In contrast, $\beta 1$ residues Val-211 and Lys-218, forming part of the AIIB2 and 4B4 epitopes, respectively, would be accessible. The epitopes of non-function-blocking mAbs (data not shown) were also fully available in this model. The exact location of the Lia1/2 epitope is not known, but it appears to lie closer to 3FN10 than the epitopes of AIIB2 and 4B4.

Only Allosteric Anti- $\beta 1$ mAbs Can Cause Complete Detachment of Fibrosarcoma Cells Pre-spread on Fibronectin—Finally, to examine the relevance of our findings to cell-surface $\alpha 5\beta 1$, we tested the ability of function-blocking anti- $\alpha 5$ and anti- $\beta 1$ mAbs to cause rounding up of HT-1080 cells pre-spread on 50K (*i.e.* with cell-surface $\alpha 5\beta 1$ in complex with ligand). The results (Fig. 11A) showed that the allosteric anti- $\beta 1$ mAbs 13, AIIB2, and 4B4 could cause complete rounding up of cells (no spread cells remaining). In contrast, the function-blocking anti- $\alpha 5$ mAbs JBS5, 16, P1D6, and SNAKA52, and the anti- $\beta 1$ mAb Lia1/2 caused only a slight reduction (typically < 25%) in the degree of cell spreading. In control experiments, run in parallel, Lia1/2 and the function-blocking anti- $\alpha 5$ mAbs were potent inhibitors of cell spreading when added to the cells before plating on 50K (Fig. 11B).

Discussion

The major findings of this report are as follows. (i) Function-blocking anti- $\alpha 5$ mAbs cannot cause dissociation of IFCs, and the epitopes of these mAbs appear to be masked in the ligand-occupied state. (ii) Allosteric function-blocking anti- $\beta 1$ mAbs (A2 class) can cause disruption of IFCs, and the epitopes of these mAbs do not appear to be masked by ligand. (iii) Members of a second group of function-blocking anti- $\beta 1$ mAbs (A1 class), which includes Lia1/2, fail to disrupt IFCs, suggesting that their epitopes are obscured in the IFC. (iv) In accord with our *in vitro* data, only allosteric mAbs could disrupt cell-surface $\alpha 5\beta 1$ -fibronectin interactions.

A preceding study defined the A1 and A2 classes of inhibitory anti- $\beta 1$ mAbs (44). From our results, it appears that the members of the A1 class are distinguished from the A2 class not only by their ability to induce cell aggregation but also by their inability to dissociate IFCs. Lia1/2 appears to have a similar

Ligand Occupancy Causes Masking of Epitopes in $\alpha 5\beta 1$

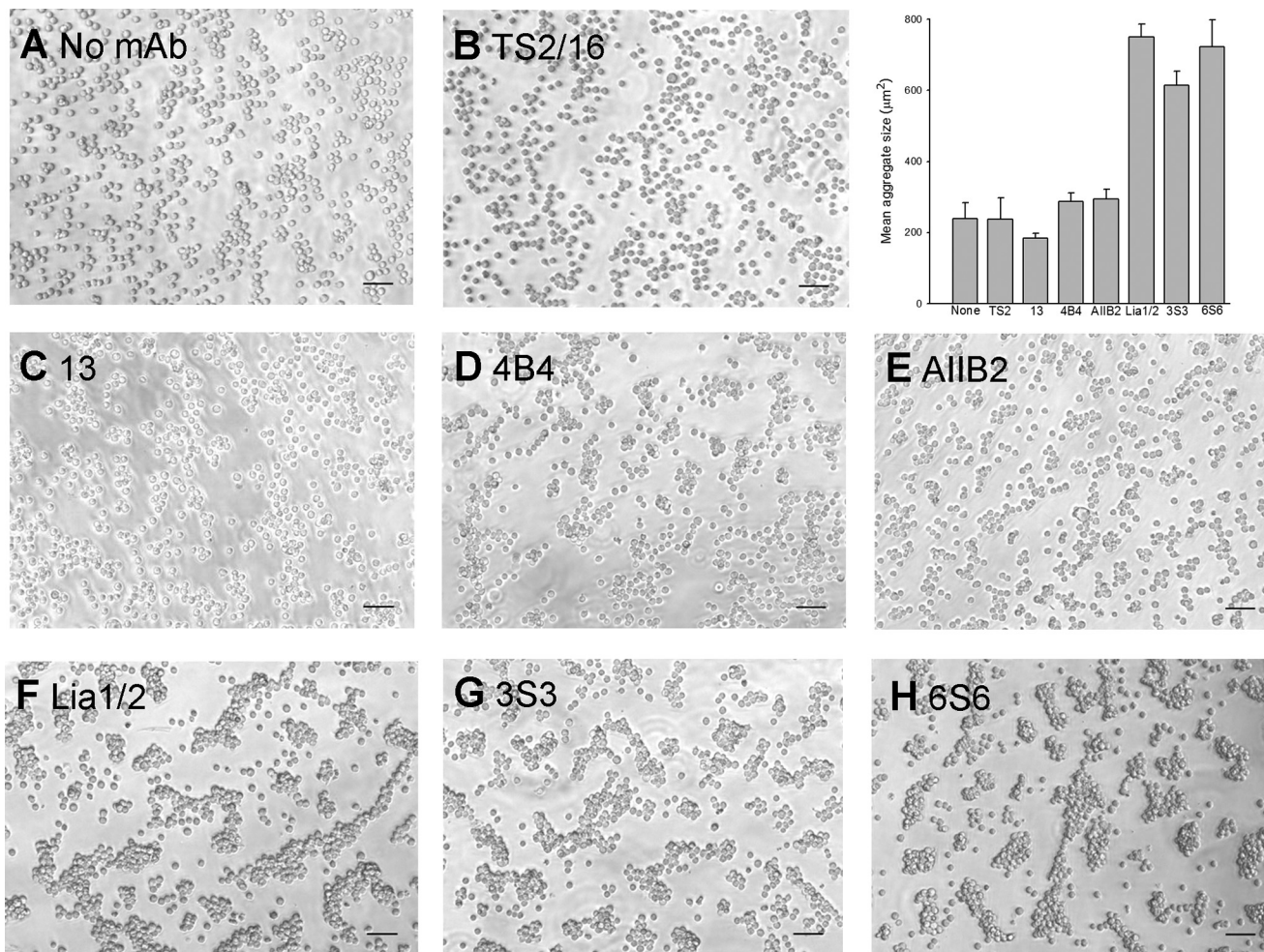


FIGURE 6. **Effect of anti- $\beta 1$ mAbs on homotypic aggregation of Jurkat cells.** A–H, cells (5×10^5 /ml) were incubated for 2 h at 37 °C in the presence of the indicated mAbs and photographed using a phase-contrast microscope. Scale bars, 50 μ m. Inset shows histogram of mean aggregate size, averaged over three fields of view (mean \pm S.D.) for no mAb (None), TS2/16 (TS2), 13, 4B4, A1B2, Lia1/2, 3S3, and 6S6. The experiment shown is representative of three separate experiments.

mode of inhibition to the function-blocking anti- $\alpha 5$ mAbs, acting in a predominantly steric, rather than allosteric, manner. The partially competitive effect of RGD peptide on Lia1/2 binding supports the notion that the Lia1/2 epitope may lie closer to the binding site of 3FN10 than the epitopes of other function-blocking anti- $\beta 1$ mAbs, leading to masking of its epitope in the IFC.

The mechanism of anti- $\beta 1$ mAb-induced cell-cell aggregation remains unclear, although previous studies (43–46) have demonstrated that this aggregation requires $\alpha 4\beta 1$ integrins. There is evidence that these mAbs induce a functional association between $\beta 1$ and CD98 and CD147 and that this complex causes intracellular signals that result in the induction of cell-cell adhesiveness (48). Similar to a previous report with the anti- $\beta 1$ mAb MEM 101A (42), C_6 -ceramide blocked the aggregation of Jurkat cells promoted by Lia1/2, 3S3, and 6S6, suggesting the involvement of similar intracellular signaling pathways by all these mAbs. Recent studies with tumor cells suggest that these pathways involve members of the PKC family (52). Elucidation of the precise mechanisms by which A1 class mAbs cause different signals to those of the A2 class will require further investigation. However, the distinct (but overlapping)

epitope location of these two classes provides a novel insight into this conundrum. Aggregation of T-cells is important *in vivo* for T-cell maturation (53); it is therefore intriguing to speculate that A1 class mAbs mimic the function of one or more natural proteins that can bind to this region of the $\beta 1$ subunit.

An important inference of our studies is that function-blocking anti-integrin subunit mAbs are not all equivalent (as has often been assumed). It is important for researchers to test several different mAbs to find the one that functions best in their specific application. Our findings demonstrate that, particularly in assays where cells or purified integrins are pre-bound to the ligand, the choice of mAb is critical. Only allosteric mAbs have the capacity to disrupt pre-existing interactions.

It could be argued that the inability of some function-blocking mAbs to perturb pre-formed cell-surface integrin-fibronectin interactions (Fig. 11A) was due to poor accessibility of these mAbs to cell adhesion sites. We consider this explanation to be unlikely because the allosteric mAbs cause complete disruption of cell spreading, and hence these mAbs must be able to access the adhesion sites. Instead, the failure of certain mAbs to markedly disrupt cell spreading appears to correlate with our *in vitro* data showing that the epitopes of these mAbs are occluded in

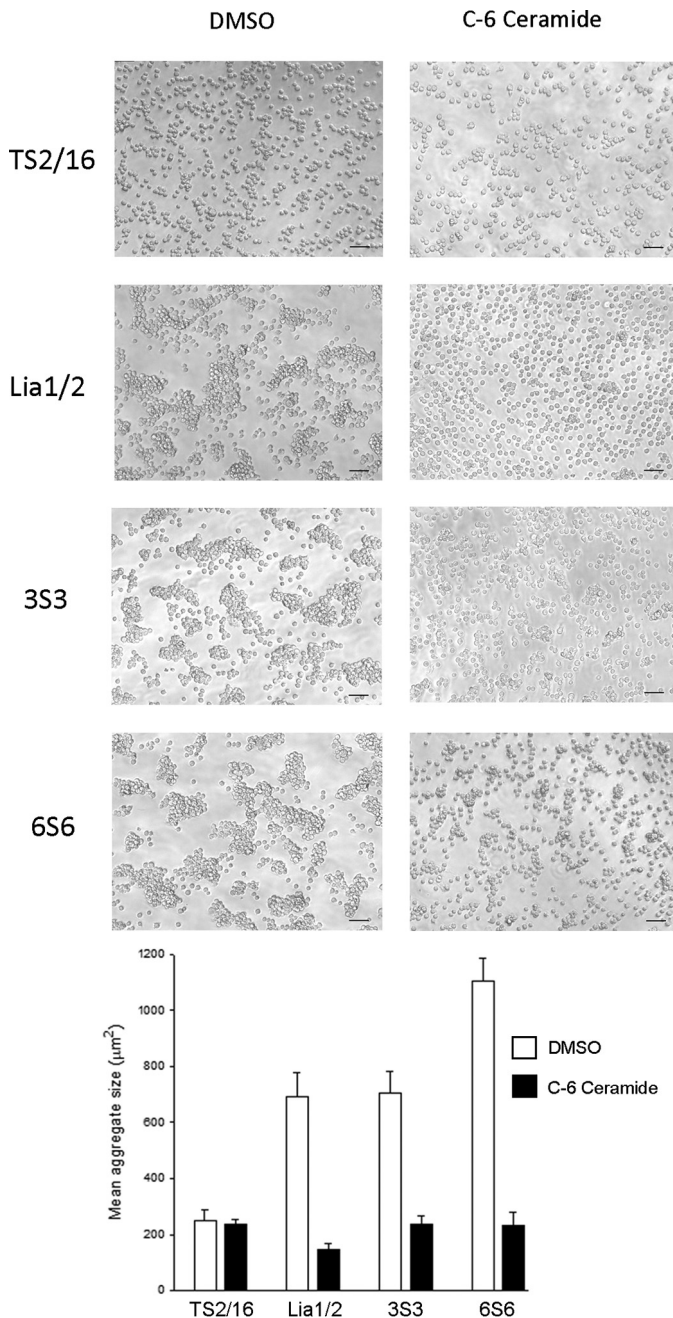


FIGURE 7. Effect of C₆-ceramide on homotypic cell aggregation stimulated by anti- $\beta 1$ mAbs. Jurkat cells (8×10^5 /ml) were incubated for 2 h at 37 °C in the presence of the indicated mAbs, in the presence of DMSO (solvent control) or 10 μ M C₆-ceramide, and photographed using a phase-contrast microscope. C₆-ceramide did not cause any reduction in cell viability over the time course of the experiment (>97% of cells were viable both before and after the experiment, as determined by propidium iodide staining, data not shown). Scale bars, 50 μ m. TS2/16 is used as a negative control mAb in this assay. Inset shows histogram of mean aggregate size, averaged over three fields of view (mean \pm S.D.). The experiment shown is representative of three separate experiments.

the IFC. A slow turnover of cell adhesion sites (which would re-expose integrin epitopes) may account for the small amount of inhibition of cell spreading by the non-allosteric inhibitory mAbs seen over the 1-h time period of the assay.

In our new model of the IFC (Figs. 9 and 10), the synergy region of 3FN9 lies very close to the residues Trp-208 and Ile-

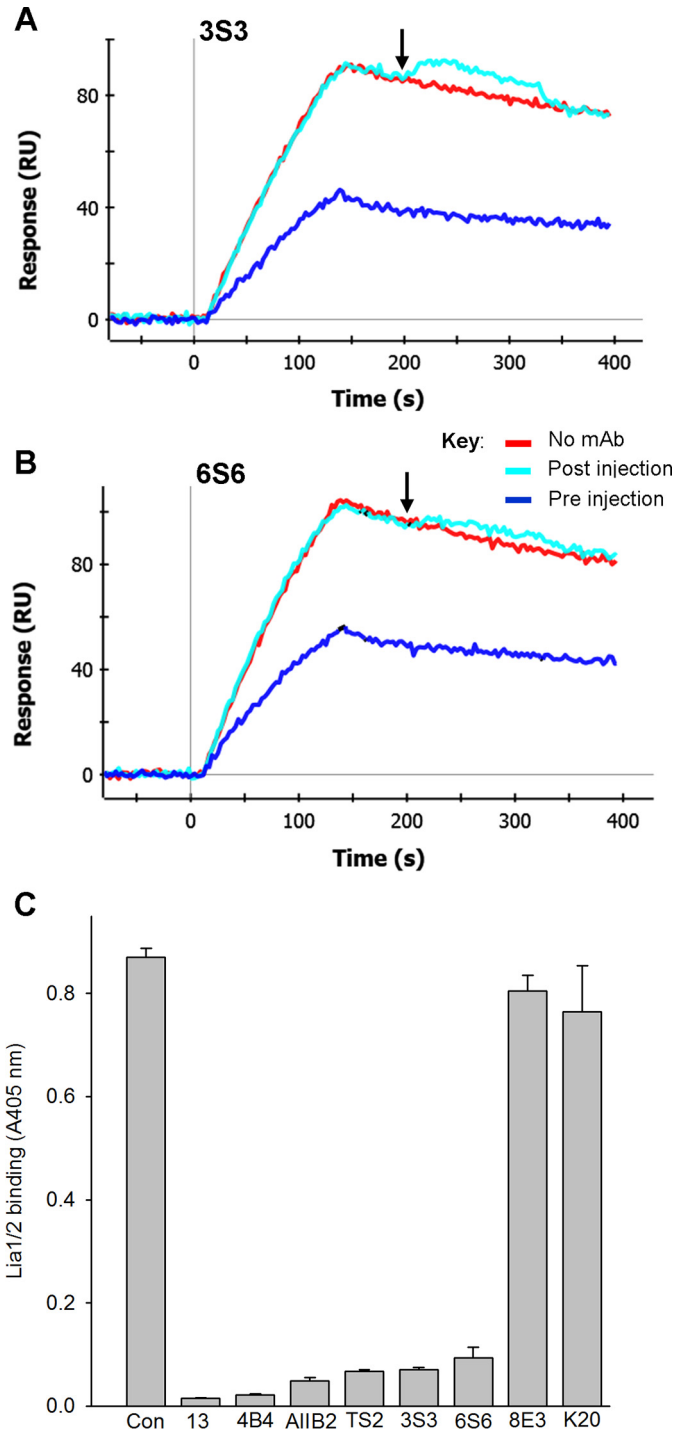


FIGURE 8. Characterization of mAbs 3S3 and 6S6. A and B, SPR test of competitive or allosteric inhibition by 3S3 and 6S6. Binding of $\alpha 5\beta 1$ -Fc to 50K fibronectin fragment took place for 120 s in three parallel channels in RB. In the blue sensorgrams, integrin was pre-mixed with 200 nM 3S3 (A) or 6S6 (B). 60 s after the start of the dissociation phase, at the time indicated by the downward-pointing arrow (~ 207 s), either RB alone (red and blue sensorgrams) or RB with 200 nM mAb (cyan sensorgrams) was injected for 120 s. C, competitive ELISA experiment to test whether epitopes of 3S3 and 6S6 overlap with that of Lia1/2. Binding of biotinylated Lia1/2 to $\alpha 5\beta 1$ -Fc was competed by a large excess of unlabeled mAbs 13, 4B4, AlIB2, 4B4, TS2/16 (TS2), 3S3, 6S6, 8E3, or K20. Con, control. Similar results were obtained in three separate experiments.

210 in the $\alpha 5$ subunit β -propeller domain, as proposed previously (15, 54). Significantly, P1D6 (whose epitope includes Leu-212) only blocks interaction of $\alpha 5\beta 1$ with fibronectin fragments

Ligand Occupancy Causes Masking of Epitopes in $\alpha 5\beta 1$

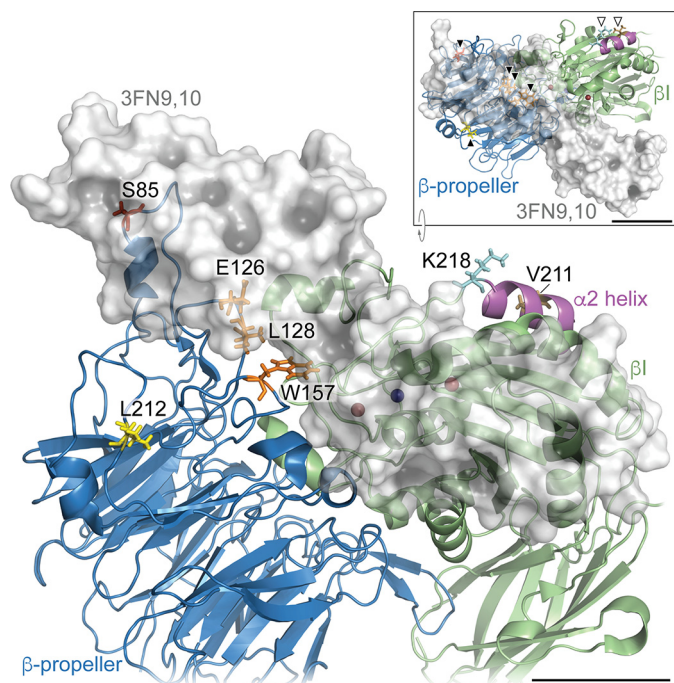


FIGURE 9. Model of headpiece region of $\alpha 5\beta 1$ bound to 3FN9,10, showing epitopes of function-blocking mAbs. In the model, the $\alpha 5$ subunit is shown as a blue ribbon, $\beta 1$ subunit as a green ribbon, and 3FN9,10 as a semi-transparent light gray surface. In the $\alpha 5$ subunit, residue Leu-212 (P1D6 epitope) is shown in yellow; residues Glu-126, Leu-128, and Trp-157 (mAb 16 epitope) are shown in orange, and residue Ser-85 (JBS5 and SNAKA52 epitopes) is shown in red. In the $\beta 1$ subunit, residues Val-211 (AIIB2 epitope) and Lys-218 (4B4 epitope) are shown in brown and cyan, respectively. The MIDAS Mg^{2+} ion is depicted as a dark blue sphere; Ca^{2+} ions at the SyMBS (synergistic metal-binding site) and ADMIDAS (adjacent to MIDAS) sites (flanking the MIDAS site) are shown as dark red spheres. The $\alpha 2$ helix in the $\beta 1$ domain is shown in magenta. Residues that contribute to the epitopes of mAbs 13, 4B4, and AIIB2 lie in the $\alpha 2$ helix (5). Inset shows an x axis-rotated view, with residues labeled in the main model indicated by arrowheads for reference ($\alpha 5$ subunit residues, black arrowheads; $\beta 1$ subunit residues, white arrowheads). Scale bars, 20 Å.

that contain the synergy region, suggesting that it binds close to a site on the $\alpha 5$ subunit that interacts with the synergy region of 3FN9 (15). Nevertheless, there has been some dispute as to whether or not the synergy region binds directly to the $\alpha 5$ subunit. For example, a lack of interaction of 3FN9 with the $\alpha 5$ subunit β -propeller domain was observed by negative staining and electron microscopy (55). In contrast, mutagenesis of $\alpha 5$ residues close to Leu-212, including Trp-208 and Ile-210, or the equivalent Trp-204 and Ile-206 in zebrafish $\alpha 5$, specifically blocks interaction of $\alpha 5\beta 1$ with fibronectin fragments that contain the synergy region (15, 54). In addition, the W204N mutation leads to loss of $\alpha 5\beta 1$ function in zebrafish development (56). Because the interaction of 3FN9 with the $\alpha 5$ subunit is weak, it could easily be disrupted by the high ionic strength conditions used for negative staining. Our new data support a direct interaction of 3FN9 with the Leu-212 region of the β -propeller because they provide evidence that the epitope of P1D6 is masked in the ligand-occupied state, and so, like the other $\alpha 5$ subunit mAbs, the epitope of P1D6 lies close to an interface between 3FN9 and the β -propeller. Binding of P1D6 to the $\alpha 5$ subunit is strongly inhibited by 3FN9-containing fragments (15), consistent with our model. An alternative model of the complex between 3FN9,10 and $\alpha 5\beta 1$ has been previously proposed by Nagae *et al.* (17), in which 3FN9,10 lies in a groove

between the α and β subunits. Our model uses the same 3FN9,10 structure as the Nagae model but incorporates new information on the position of 3FN10 (49) to direct the orientation of 3FN9. In the Nagae model, although the epitope residues of mAbs JBS5, SNAKA52, and 16 would still be predicted to be obscured by fibronectin binding, the P1D6 epitope residue Leu-212 would be minimally masked. The principle of epitope occlusion used here could also be utilized in other receptor-ligand systems to help define the boundary of the receptor-ligand interface.

A recent study of the location of epitopes in integrin α subunits identified the 4-1 loop of β -propeller blade 2 (which in $\alpha 5$ contains the JBS5 and SNAKA52 epitopes) and the 3-4 loop of β -propeller blade 3 (P1D6 epitope in $\alpha 5$) as the site of >80% of function-blocking mAb epitopes (29). Hence, the results of our study are likely to be applicable to a large proportion of other α subunit mAbs, *i.e.* epitope masking by ligand occupancy is likely to be a common feature in other integrins.

Accordingly, it is important to note that the epitopes of some therapeutic anti-integrin mAbs, such as the anti- $\alpha 4$ mAb Tysabri/natalizumab and the anti- αV mAb 17E6, may be partly obscured in the ligand-occupied state (30, 31). Consequently, complete blockade of integrin function by these biologicals would be dependent on turnover of integrin-ligand complexes to re-expose integrin epitopes, and this turnover can be very slow (35, 57–60). For example, we previously observed that $\alpha 5\beta 1$ -fibronectin complexes gradually transition to a very long-lived state, $k_{off} \sim 10^{-5} s^{-1}$, *i.e.* $t_{1/2} \sim 19$ h (35). Our study suggests that epitope masking could reduce the effectiveness of drugs like Tysabri, and in the future it will be important to test whether their efficacy could be enhanced by co-administration of an allosteric inhibitor. Epitope masking could also have contributed to the lack of efficacy of some blocking anti-integrin mAbs in clinical trials (7–9).

In summary, our findings re-emphasize the importance of allosteric inhibition for effective blockade of integrin function (35). Allosteric anti- $\beta 1$ mAbs such as AIIB2 are already showing therapeutic potential for radiosensitization of tumors and prevention of metastasis (61–63). Finally, ligand-induced epitope masking may occur in other receptor-ligand systems, and in the future it will be important to address whether this phenomenon limits the efficacy of non-integrin function-blocking therapeutic mAbs.

Experimental Procedures

Materials—The production of recombinant integrin $\alpha 5\beta 1$ -Fc has been previously described (38). In brief, $\alpha 5\beta 1$ -Fc was produced in NS0 cells and purified from culture medium using protein A-Sepharose. mAb TS2/16 was a gift from F. Sánchez-Madrid (Hospital de la Princesa, Madrid, Spain); mAbs JB1A, 3S3, and 6S6 were gifts from J. A. Wilkins (University of Manitoba, Winnipeg, Manitoba, Canada); and mAbs 11, 13, and 16 were gifts from K. M. Yamada (National Institutes of Health, Bethesda). 4B4 was from Beckman Coulter (UK). SNAKA51, 8E3, and SNAKA52 have been previously described (39–40, 64). P1D6, AIIB2, and HUTS-4 were from Merck Millipore (UK). VC5 and JBS5 were purchased from Pharmingen and Serotec (UK), respectively. K20 was a gift from P. T. Caswell (University of Manchester, Man-

Ligand Occupancy Causes Masking of Epitopes in $\alpha 5\beta 1$

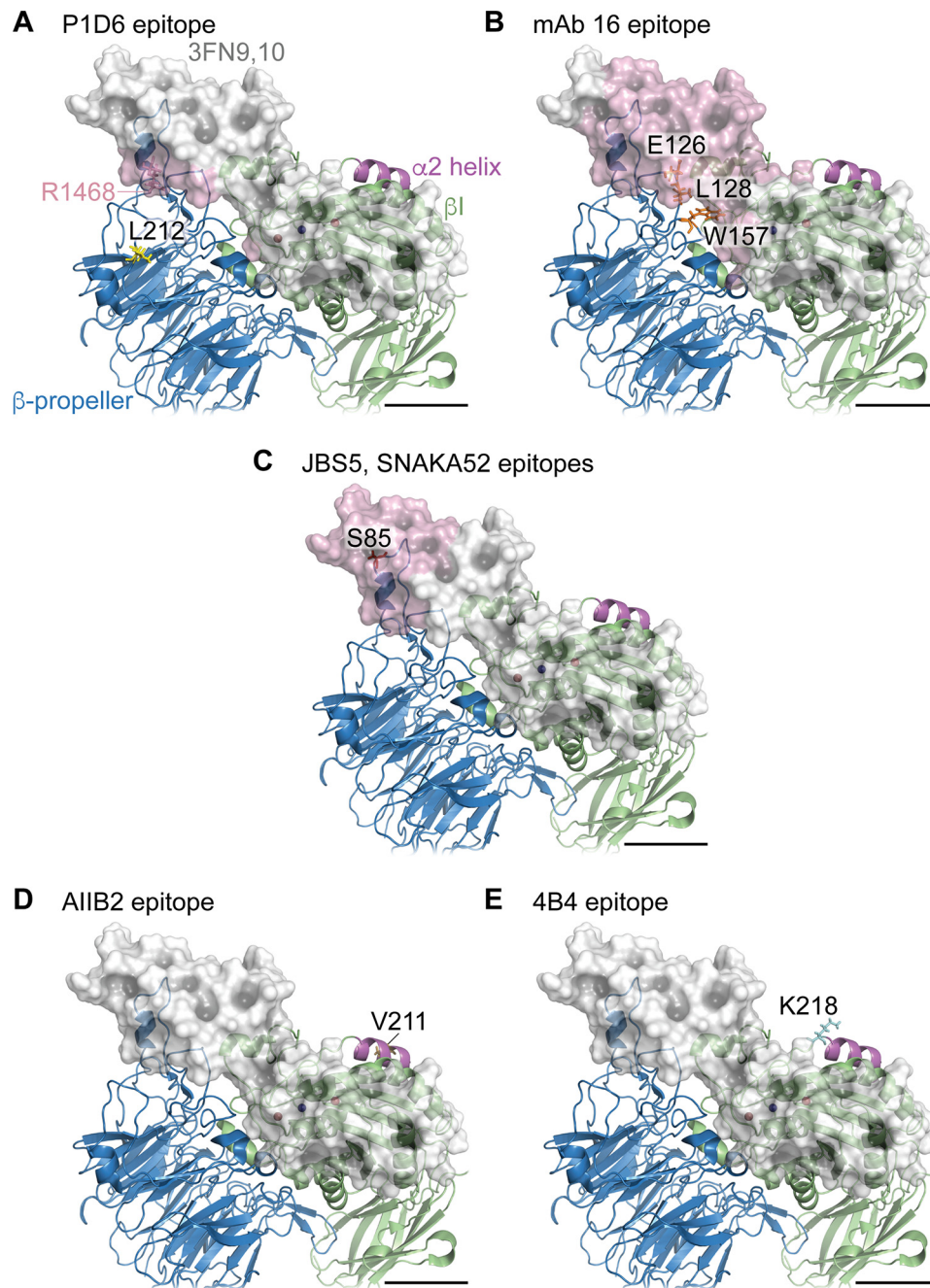


FIGURE 10. **Putative accessibility of epitopes of function-blocking mAbs in a model of the headpiece of $\alpha 5\beta 1$ bound to 3FN9,10.** A–E, molecular model is the same as that shown in Fig. 9. In respective panels, residue Leu-212 (P1D6 epitope) is shown in yellow; residues Glu-126, Leu-128, and Trp-157 (mAb 16 epitope) are shown in orange; residue Ser-85 (JBS5 and SNAKA52 epitopes) is shown in red within the $\alpha 5$ subunit (blue ribbon); residue Val-211 (AIIB2 epitope) is shown in brown, and residue Lys-218 (4B4 epitope) is shown in cyan within the $\beta 1$ subunit (green ribbon). The $\alpha 2$ helix in the $\beta 1$ domain is shown in magenta. 3FN9,10 is shown as a semi-transparent light gray surface, and the surface of accessible 3FN9,10 residues within 20 Å of indicated mAb epitope residues is rendered in semi-transparent pink. Residue Arg-1468 (from the Pro-Pro-Ser-Arg-Asn synergy sequence of murine fibronectin) is shown in dark pink and indicated by the pink text in A. Anti- $\alpha 5$ mAbs would be sterically hindered from binding to indicated epitope residues by fibronectin, whereas anti- $\beta 1$ mAbs would not. Scale bars, 20 Å.

chester, UK), and Lia1/2 was from Biorbyt (UK). For competitive ELISAs, Lia1/2 was biotinylated using sulfo-*N*-hydroxysuccinimide-LC-biotin (64). Further details of all the mAbs used in this study are shown in Table 1.

The 50-kDa cell-binding domain fragment of human fibronectin (3FN6–10, 50K) and the inactive mutant (50K-KGE) were produced in *Escherichia coli* and purified as before (15, 16). 50K and 50K-KGE were biotinylated and purified by

gel filtration as described previously (35). Both proteins contain a single site for biotinylation in 3FN7. Avidin (from egg white) was obtained from Life Technologies, Inc. Peptide GCRGD-SPCG (cRGD) was purchased from Peptide 2.0, Inc., and cyclized by oxidation as described previously (16). *N*-Hexanoyl-D-sphingosine (C_6 -ceramide), ExtrAvidin peroxidase, bovine serum albumin (BSA), and mouse IgG were purchased from Sigma.

Ligand Occupancy Causes Masking of Epitopes in $\alpha 5\beta 1$

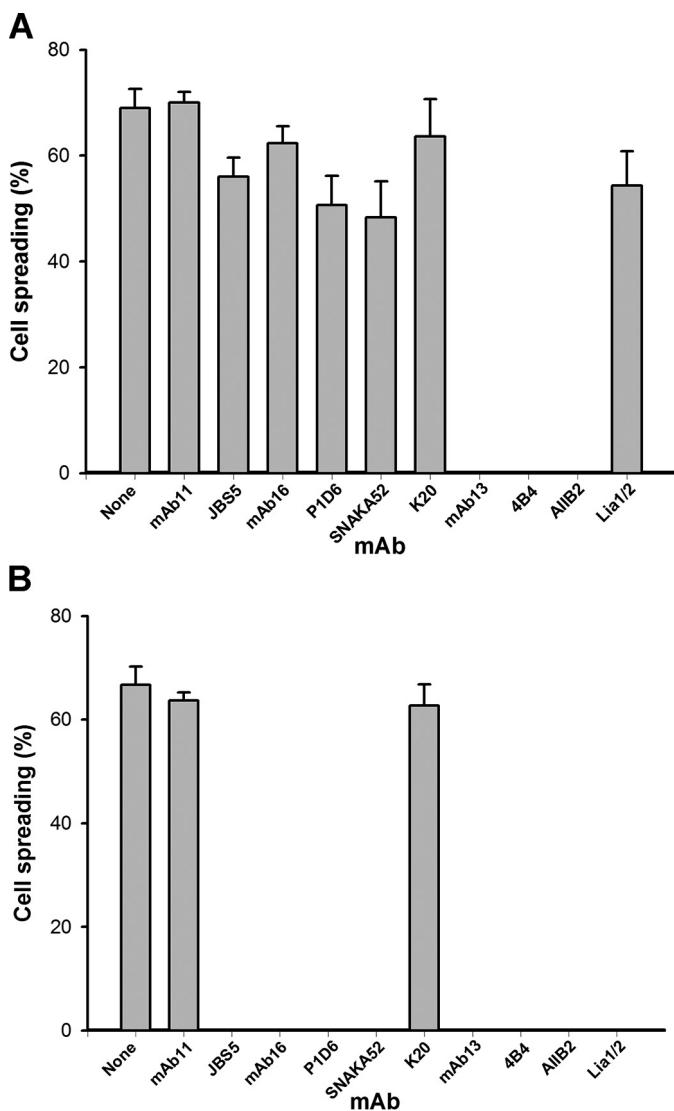


FIGURE 11. *A*, effect of function-blocking mAbs on HT-1080 cells pre-spread on 50K. Cells were allowed to spread on 50K for 1 h and then exposed to the indicated anti- $\alpha 5$ (JB55, 16, P1D6, or SNAKA52) or anti- $\beta 1$ (13, 4B4, AlIB2, or Lia1/2) mAbs for 1 h. The percentage of spread cells was then quantitated. The non-function-blocking anti- $\alpha 5$ mAb 11 and anti- $\beta 1$ mAb K20 were used as controls. *B*, effect of the same mAbs in an assay in which the mAbs were added to the cells before spreading on 50K. Similar results were obtained in three separate experiments.

SPR—Experiments were performed using the ProteOn XPR36 instrument (Bio-Rad). Running buffer (RB) was 150 mM NaCl, 10 mM HEPES, 0.05% (w/v) Tween 20, pH 7.4, with 1 mM MnCl₂. Immobilization of avidin was performed on a GLC chip (Bio-Rad) in the vertical orientation. Two channels were activated with 150 μ l of a 1:1 mixture of 20 mM *N*-ethyl-*N'*-(3-dimethylaminopropyl)carbodiimide and 11 mM sulfo-*N*-hydroxysuccinimide in water at a flow rate of 30 μ l/min. Avidin was diluted in RB to a final concentration of 1.2 μ M, and 150 μ l was injected, followed by an injection of 150 μ l of 1 M ethanolamine-HCl, pH 8.5, at a flow rate of 30 μ l/min. The immobilization level of avidin was \sim 3200 resonance units. Next, 150 μ l of biotinylated 50K-KGE in one vertical channel and biotinylated 50K in the second (20–200 nM) in RB were injected to allow their capture by the immobilized avidin. Injection of 50K

and 50K-KGE was repeated as necessary to give equivalent immobilization levels of the two proteins. The 50K-KGE channel was used as a reference. Final immobilization levels were in the range 100–300 resonance units. All experiments were performed at 25 $^{\circ}$ C.

To test the effect of mAbs on the dissociation rate of integrin-50K complexes, 100 μ l of $\alpha 5\beta 1$ -Fc in RB was injected in three parallel horizontal channels at 50 μ l/min, and binding to 50K was allowed to occur for 120 s, followed by injection of RB for 60 s. Next, either RB alone (channel 1) or RB with 100 nM mAb (channel 2) was injected for 120 s, followed by a return to RB alone. In channel 3, $\alpha 5\beta 1$ -Fc was pre-mixed with 100 nM mAb before injection onto the chip. The three-stage injection described above (integrin-buffer-buffer or integrin-buffer-mAb) was accomplished using the “Coinject Analyte” command. Injection quality was set at “maximum.” The integrin concentration used was 6 nM. In experiments with 3S3 and 6S6, the concentration of mAb was 200 nM and integrin concentration was 3 nM. The concentrations of mAb used gave a maximal effect in the assays.

All binding sensorgrams were collected, processed, and analyzed using the integrated ProteOn Manager software (Bio-Rad). Short black segments on some sensorgrams represent artifact (spike) removal from the data. Dissociation rates (k_{off}) were calculated using off-rate analysis (ProteOn Manager software) using Equation 1,

$$A = A_0 \times \exp(-k_{\text{off}} \times (t - t_0)) \quad (\text{Eq. 1})$$

where A_0 = binding at time t_0 . All results shown are representative of at least three separate experiments.

Epitope Mapping of Lia1/2—Mapping of the Lia1/2 epitope was performed essentially as described previously for other function-perturbing anti- $\beta 1$ mAbs (32, 41). The M287V human-to-mouse mutation was made in human $\beta 1$ -GFP (65) using the QuickChange XL mutagenesis kit (Agilent Technologies) according to the manufacturer’s instructions. CHO-K1 cells were transiently transfected with either wild-type or mutant integrin by nucleofection (Lonza), and the binding of Lia1/2 was detected by flow cytometry using an LSR Fortessa cytometer (BD Biosciences) with AlexaFluor 647 anti-mouse IgG (Strattech) as secondary antibody after gating the cells for those expressing GFP. These assays were repeated twice, with the same overall results.

Effect of 50K and cRGD on mAb Binding—Purified $\alpha 5\beta 1$ -Fc was diluted 1:1000 with Dulbecco’s PBS (final concentration \sim 2 μ g/ml), and 50- μ l aliquots were added to the wells of a 96-well ELISA plate (Costar $\frac{1}{2}$ -volume). Plates were incubated overnight at room temperature, and wells were blocked for 1–3 h with 200 μ l of 5% (w/v) BSA, 150 mM NaCl, 0.05% (w/v) NaN₃, 25 mM Tris-HCl, pH 7.4. Wells were then washed three times with 200 μ l of 150 mM NaCl, 25 mM Tris-HCl, pH 7.4, containing 1 mg/ml BSA (buffer A) with 1 mM MnCl₂. mAbs (0.1 μ g/ml) in buffer A with 1 mM MnCl₂ were added to the wells in the presence of varying concentrations of cRGD or 50K. The plate was then incubated at room temperature for 2 h. Unbound antibody was aspirated, and the wells were washed three times with buffer A. Bound antibody was quantified by

addition of 1:1000 dilution of goat anti-mouse or anti-rat peroxidase conjugate (Jackson ImmunoResearch) in buffer A with 1 mM MnCl_2 for 30 min at room temperature. Wells were then washed four times with buffer A, and color was developed using 2,2'-azino-bis(3-ethylbenzothiazoline-6-sulfonic acid) substrate. Measurements obtained were the means \pm S.D. of four replicate wells. Experiments examining the effect of varying concentrations of cRGD on the binding of Lia1/2 at 0.05 and 0.5 $\mu\text{g}/\text{ml}$ were performed in the same manner.

Competitive ELISA—ELISA plates were coated with $\alpha 5\beta 1$ -Fc, blocked, and washed as described above. Biotinylated Lia1/2 (0.1 $\mu\text{g}/\text{ml}$) in buffer A was added to the wells in the absence or presence of a large excess of unlabeled competitor mAbs (10 or 30 $\mu\text{g}/\text{ml}$ for 3S3 and 6S6). The plate was then incubated at room temperature for 2 h. Unbound antibodies were aspirated, and the wells were washed three times with buffer A. Bound biotinylated antibody was quantified by the addition of 1:500 dilution of ExtrAvidin peroxidase conjugate in buffer A for 30 min at room temperature. Wells were then washed four times with buffer A, and color was developed using 2,2'-azino-bis(3-ethylbenzothiazoline-6-sulfonic acid) substrate. Measurements obtained were the means \pm S.D. of four replicate wells. In all the plate assays described above, the amount of nonspecific binding was measured by determining the level of antibody binding to wells coated with BSA alone; these values were subtracted from the corresponding values for receptor-coated wells. Each experiment shown is representative of at least three separate experiments.

Cell Aggregation Assays—Jurkat cells were maintained in complete RPMI 1640 medium (supplemented with 2 mM glutamine and 10% fetal bovine serum). Aggregation assays were performed essentially as described by Lee *et al.* (42). Cells ($5 \times 10^5/\text{ml}$) were incubated in medium alone or in medium with mAbs (1 $\mu\text{g}/\text{ml}$) in a 96-well plate (Costar). After a 2-h incubation, cells were photographed with an inverted light microscope (Leica DM IL) equipped with a Leica DFC295 video camera. The mean aggregate size of three independent fields of view was quantified in ImageJ (66) by converting each image to binary and using the “analyze particles” function to measure the size of each aggregate in the field. Results are presented as mean \pm S.D. of mean aggregate size over the three fields.

For inhibition experiments, cells were pre-incubated with 10 μM C_6 -ceramide or an equivalent volume of solvent (DMSO) only for 1 h at 37 °C before addition of the mAbs (42). All results shown are representative of three separate experiments.

Molecular Modeling—To model the position of 3FN9,10 bound to the headpiece of $\alpha 5\beta 1$, the superposition of the crystal structures of the RGD-bound $\alpha 5\beta 1$ (Protein Data Bank code 4WK4, with RGD peptide removed) (18) and the $\alpha V\beta 3$ -3FN10 complex (Protein Data Bank code 4MMX) (49) was generated using PyMOL (version 1.7.2.3; Schrödinger, LLC). The NMR structure of 3FN9,10 (Protein Data Bank code 2MFN; model 10) (50) was docked onto $\alpha 5\beta 1$ by alignment with 3FN10 of the $\alpha V\beta 3$ -3FN10 complex. The obminimize function in Open Babel (version 2.3.1) (67) was used to confirm geometry optimization and energy minimization for the aligned molecules. Images were rendered in PyMOL and assembled using Illustra-

tor (version CS6; Adobe). A video representation of the model was generated in PyMOL.

Cell Spreading Assays—HT-1080 fibrosarcoma cells were maintained in complete Dulbecco's modified Eagle's medium supplemented with 2 mM glutamine and 10% fetal bovine serum. Wells of a 96-well plate (Costar) were coated with 50K (2 $\mu\text{g}/\text{ml}$ in Dulbecco's PBS) for 60 min at room temperature, and then sites on the plastic for nonspecific cell adhesion were blocked for 30 min at room temperature with 100 μl of 10 mg/ml heat-denatured BSA. HT-1080 cells were detached with 0.05% trypsin, 0.02% EDTA, resuspended to $5 \times 10^5/\text{ml}$ in serum-free Dulbecco's minimal essential medium with 25 mM HEPES, and allowed to recover for 10 min at 37 °C. Cells were then added to the wells and allowed to spread for 60 min in a humidified atmosphere of 5% CO_2 at 37 °C. mAbs were then added to wells to a final concentration of 10 $\mu\text{g}/\text{ml}$, and the cells were incubated for a further 60 min. The cells were then fixed with 3% glutaraldehyde, and the degree of spreading was quantified using phase-contrast microscopy. Each data point (mean \pm S.D.) was obtained by counting three sets of 100 cells/well from a number of randomly selected fields. In a parallel assay, mAbs were added to the cells at the same time as plating on 50K. No cell spreading was observed on wells coated only with heat-denatured BSA.

Author Contributions—A. P. M. performed the SPR, ligand inhibition, and competitive ELISA experiments, designed the project, and wrote most of the manuscript. J. A. A. performed the SDS-PAGE, cell aggregation assays, the M287V mutant FACS analysis, and the cell spreading assays. A. B. performed the molecular modeling and helped with figure preparation. Y. T. performed the Lia1/2 epitope mapping experiments. T. A. J., M. J. H., and the other authors reviewed the results and contributed to manuscript preparation.

Acknowledgments—We thank J. Popplewell for helpful discussions; J. D. Humphries for comments on the manuscript; and J. A. Wilkins, F. Sánchez-Madrid, P. T. Caswell, and K. M. Yamada for antibodies. We are grateful to H. D. Ruis Nivia for assistance with purification of biotinylated Lia1/2 and fibronectin fragments and M. Jackson for help with FACS.

References

- Hynes, R. O. (2002) Integrins: bidirectional, allosteric signalling machines. *Cell* **110**, 673–687
- Goodman, S. L., and Picard, M. (2012) Integrins as therapeutic targets. *Trends Pharmacol. Sci.* **33**, 405–412
- Blandin, A. F., Renner, G., Lehmann, M., Lelong-Rebel, I., Martin, S., and Dontenwill, M. (2015) $\beta 1$ integrins as therapeutic targets to disrupt hallmarks of cancer. *Front. Pharmacol.* **6**, 279
- Giordano, A., Musumeci, G., D'Angelillo, A., Rossini, R., Zoccai, G. B., Messina, S., Coscioni, E., Romano, S., and Romano, M. F. (2016) Effects of glycoprotein IIb/IIIa antagonists: anti platelet aggregation and beyond. *Curr. Drug Metab.* **17**, 194–203
- Rice, G. P., Hartung, H. P., and Calabresi, P. A. (2005) Anti- $\alpha 4$ integrin therapy for multiple sclerosis: mechanisms and rationale. *Neurology* **64**, 1336–1342
- Cherry, L. N., Yunker, N. S., Lambert, E. R., Vaughan, D., and Lowe, D. K. (2015) Vedolizumab: an $\alpha 4\beta 7$ integrin antagonist for ulcerative colitis and Crohn's disease. *Ther. Adv. Chronic Dis.* **6**, 224–233
- Hersey, P., Sosman, J., O'Day, S., Richards, J., Bedikian, A., Gonzalez, R., Sharfman, W., Weber, R., Logan, T., Buzoianu, M., Hammershaimb, L.,

Ligand Occupancy Causes Masking of Epitopes in $\alpha 5\beta 1$

- Kirkwood, J. M., and Etaracizumab Melanoma Study Group. (2010) A randomized phase 2 study of etaracizumab, a monoclonal antibody against integrin $\alpha V\beta 3$ + or - dacarbazine in patients with stage IV metastatic melanoma. *Cancer* **116**, 1526–1534
- Mateo, J., Berlin, J., de Bono, J. S., Cohen, R. B., Keedy, V., Mugundu, G., Zhang, L., Abbattista, A., Davis, C., Gallo Stampino, C., and Borghaei, H. (2014) A first-in-human study of the anti- $\alpha 5\beta 1$ integrin monoclonal antibody PF-04605412 administered intravenously to patients with advanced solid tumors. *Cancer Chemother. Pharmacol.* **74**, 1039–1046
 - Heidenreich, A., Rawal, S. K., Szkarlat, K., Bogdanova, N., Dirix, L., Stenzl, A., Welslau, M., Wang, G., Dawkins, F., de Boer, C. J., and Schrijvers, D. (2013) A randomized, double-blind, multicenter, phase 2 study of a human monoclonal antibody to human αV integrins (intetumumab) in combination with docetaxel and prednisone for the first-line treatment of patients with metastatic castration-resistant prostate cancer. *Ann. Oncol.* **24**, 329–336
 - Xiong, J. P., Stehle, T., Diefenbach, B., Zhang, R., Dunker, R., Scott, D. L., Joachimiak, A., Goodman, S. L., and Arnaout, M. A. (2001) Crystal structure of the extracellular segment of integrin $\alpha V\beta 3$. *Science* **294**, 339–345
 - Xiao, T., Takagi, J., Collier, B. S., Wang, J. H., and Springer, T. A. (2004) Structural basis for allostery in integrins and binding to fibrinogen-mimetic therapeutics. *Nature* **432**, 59–67
 - Xiong, J.-P., Stehle, T., Zhang, R., Joachimiak, A., Frech, M., Goodman, S. L., and Arnaout, M. A. (2002) Crystal structure of the extracellular segment of integrin $\alpha V\beta 3$ in complex with an Arg-Gly-Asp ligand. *Science* **296**, 151–155
 - Irie, A., Kamata, T., and Takada, Y. (1997) Multiple loop structures critical for ligand binding of the integrin $\alpha 4$ subunit in the upper face of the β -propeller model. *Proc. Natl. Acad. Sci. U.S.A.* **94**, 7198–7203
 - Kamata, T., Tieu, K. K., Irie, A., Springer, T. A., and Takada, Y. (2001) Amino acid residues in the $\alpha 1$ subunit that are critical for ligand binding to integrin $\alpha 1\beta 3$ are clustered in the β -propeller model. *J. Biol. Chem.* **276**, 44275–44283
 - Mould, A. P., Askari, J. A., Aota Si, Yamada, K. M., Irie, A., Takada, Y., Mardon, H. J., and Humphries, M. J. (1997) Defining the topology of integrin $\alpha 5\beta 1$ -fibronectin interactions using inhibitory anti- $\alpha 5$ and anti- $\beta 1$ monoclonal antibodies—evidence that the synergy sequence of fibronectin is recognized by the NH_2 -terminal repeats of the $\alpha 5$ subunit. *J. Biol. Chem.* **272**, 17283–17292
 - Mould, A. P., Koper, E. J., Byron, A., Zahn, G., and Humphries, M. J. (2009) Mapping the ligand-binding pocket of integrin $\alpha 5\beta 1$ using a gain-of-function approach. *Biochem. J.* **424**, 179–189
 - Nagae, M., Re, S., Mihara, E., Nogi, T., Sugita, Y., and Takagi, J. (2012) Crystal structure of $\alpha 5\beta 1$ integrin ectodomain: atomic details of the fibronectin receptor. *J. Cell Biol.* **197**, 131–140
 - Xia, W., and Springer, T. A. (2014) Metal ion and ligand binding of integrin $\alpha 5\beta 1$. *Proc. Natl. Acad. Sci. U.S.A.* **111**, 17863–17868
 - Aota, S., Nomizu, M., and Yamada, K. M. (1994) The short amino acid sequence Pro-His-Ser-Arg-Asn in human fibronectin enhances cell-adhesive function. *J. Biol. Chem.* **269**, 24756–24761
 - Luo, B. H., Carman, C. V., and Springer, T. A. (2007) Structural basis of integrin regulation and signaling. *Annu. Rev. Immunol.* **25**, 619–647
 - Askari, J. A., Buckley, P. A., Mould, A. P., and Humphries, M. J. (2009) Linking integrin conformation to function. *J. Cell Sci.* **122**, 165–170
 - Zhu, J., Zhu, J., and Springer, T. A. (2013) Complete integrin headpiece opening in eight steps. *J. Cell Biol.* **201**, 1053–1068
 - Mould, A. P., Askari, J. A., Barton, S., Kline, A. D., McEwan, P. A., Craig, S. E., and Humphries, M. J. (2002) Integrin activation involves a conformational change in the $\alpha 1$ helix of the β subunit A-domain. *J. Biol. Chem.* **277**, 19800–19805
 - Mould, A. P., Barton, S. J., Askari, J. A., McEwan, P. A., Buckley, P. A., Craig, S. E., and Humphries, M. J. (2003) Conformational changes in the integrin βA domain provide a mechanism for signal transduction via hybrid domain movement. *J. Biol. Chem.* **278**, 17028–17035
 - Barton, S. J., Travis, M. A., Askari, J. A., Buckley, P. A., Craig, S. E., Humphries, M. J., and Mould, A. P. (2004) Novel activating and inactivating mutations in the integrin $\beta 1$ subunit A domain. *Biochem. J.* **380**, 401–407
 - Zhang, C., Liu, J., Jiang, X., Haydar, N., Zhang, C., Shan, H., and Zhu, J. (2013) Modulation of integrin activation and signaling by $\alpha 1/\alpha 1'$ -helix unbending at the junction. *J. Cell Sci.* **126**, 5735–5747
 - Burrows, L., Clark, K., Mould, A. P., and Humphries, M. J. (1999) Fine mapping of inhibitory anti- $\alpha 5$ monoclonal antibody epitopes that differentially affect integrin-ligand binding. *Biochem. J.* **344**, 527–533
 - Humphries, M. J., Symonds, E. J., and Mould, A. P. (2003) Mapping functional residues onto integrin crystal structures. *Curr. Opin. Struct. Biol.* **13**, 236–243
 - Nishimichi, N., Kawashima, N., and Yokosaki, Y. (2015) Epitopes in $\alpha 8\beta 1$ and other RGD-binding integrins delineate classes of integrin-blocking antibodies and major binding loops in α subunits. *Sci. Rep.* **5**, 13756
 - Mahalingam, B., Van Agthoven, J. F., Xiong, J. P., Alonso, J. L., Adair, B. D., Rui, X., Anand, S., Mehrbod, M., Mofrad, M. R., Burger, C., Goodman, S. L., and Arnaout, M. A. (2014) Atomic basis for the species-specific inhibition of αV integrins by mAb 17E6 is revealed by the crystal structure of $\alpha V\beta 3$ ectodomain-17E6 Fab complex. *J. Biol. Chem.* **289**, 13801–13809
 - Yu, Y., Schürpf, T., and Springer, T. A. (2013) How natalizumab binds and antagonizes $\alpha 4$ integrins. *J. Biol. Chem.* **288**, 32314–32325
 - Takada, Y., and Puzon, W. (1993) Identification of a regulatory region of integrin $\beta 1$ subunit using activating and inhibiting antibodies. *J. Biol. Chem.* **268**, 17597–17601
 - Byron, A., Humphries, J. D., Askari, J. A., Craig, S. E., Mould, A. P., and Humphries, M. J. (2009) Anti-integrin monoclonal antibodies. *J. Cell Sci.* **122**, 4009–4011
 - Yu, Y., Zhu, J., Mi, L. Z., Walz, T., Sun, H., Chen, J.-F., and Springer, T. A. (2012) Structural specializations of $\alpha 4\beta 7$, an integrin that mediates rolling adhesion. *J. Cell Biol.* **196**, 131–146
 - Mould, A. P., Craig, S. E., Byron, S. K., Humphries, M. J., and Jowitt, T. A. (2014) Disruption of integrin-fibronectin complexes by allosteric but not ligand-mimetic inhibitors. *Biochem. J.* **464**, 301–313
 - Reardon, D. A., and Cheresch, D. (2011) Cilengitide: a prototypic integrin inhibitor for the treatment of glioblastoma and other malignancies. *Genes Cancer* **2**, 1159–1165
 - Mason, W. P. (2015) End of the road: confounding results of the CORE trial terminate the arduous journey of cilengitide for glioblastoma. *Neuro. Oncol.* **17**, 634–635
 - Coe, A. P., Askari, J. A., Kline, A. D., Robinson, M. K., Kirby, H., Stephens, P. E., and Humphries, M. J. (2001) Generation of a minimal $\alpha 5\beta 1$ integrin-Fc fragment. *J. Biol. Chem.* **276**, 35854–35866
 - Clark, K., Pankov, R., Travis, M. A., Askari, J. A., Mould, A. P., Craig, S. E., Newham, P., Yamada, K. M., and Humphries, M. J. (2005) A specific $\alpha 5\beta 1$ -integrin conformation promotes directional integrin translocation and fibronectin matrix formation. *J. Cell Sci.* **118**, 291–300
 - Mould, A. P., Travis, M. A., Barton, S. J., Hamilton, J. A., Askari, J. A., Craig, S. E., Macdonald, P. R., Kammerer, R. A., Buckley, P. A., and Humphries, M. J. (2005) Evidence that monoclonal antibodies directed against the integrin β subunit plexin/semaphorin/integrin domain stimulate function by inducing receptor extension. *J. Biol. Chem.* **280**, 4238–4246
 - Mould, A. P., Akiyama, S. K., and Humphries, M. J. (1996) The inhibitory anti- $\beta 1$ integrin monoclonal antibody 13 recognizes an epitope that is attenuated by ligand occupancy. Evidence for allosteric inhibition of integrin function. *J. Biol. Chem.* **271**, 20365–20374
 - Lee, Y. G., Lee, J., and Cho, J. Y. (2010) Cell-permeable ceramides act as novel regulators of U937 cell-cell adhesion mediated by CD29, CD98, and CD147. *Immunobiology* **215**, 294–303
 - Campanero, M. R., Pulido, R., Ursa, M. A., Rodríguez-Moya, M., de Landázuri, M. O., and Sánchez-Madrid, F. (1990) An alternative leukocyte homotypic adhesion mechanism, LFA-1/ICAM-1 independent, triggered through the human VLA-4 integrin. *J. Cell Biol.* **110**, 2157–2165
 - Campanero, M. R., Arroyo, A. G., Pulido, R., Ursa, A., de Matías, M. S., Sánchez-Mateos, P., Kassner, P. D., Chan, B. M., Hemler, M. E., Corbí, A. L., de Landázuri, M. O., and Sánchez-Madrid, F. (1992) Functional role of $\alpha 2\beta 1$ and $\alpha 4\beta 1$ integrins in leukocyte intercellular adhesion induced through the common $\beta 1$ subunit. *Eur. J. Immunol.* **22**, 3111–3119
 - Shen, C. X., Stewart, S., Wayner, E., Carter, W., and Wilkins, J. (1991) Antibodies to different members of the $\beta 1$ (CD29) integrins induce ho-

- motypic and heterotypic cellular aggregation. *Cell. Immunol.* **138**, 216–228
46. Muñoz, M., Serrador, J., Sánchez-Madrid, F., and Teixidó, J. (1996) A region of the integrin VLA $\alpha 4$ subunit involved in homotypic cell aggregation and in fibronectin but not vascular cell adhesion molecule-1 binding. *J. Biol. Chem.* **271**, 2696–2702
 47. Wilkins, J. A., Li, A., Ni, H., Stupack, D. G., and Shen, C. (1996) Control of $\beta 1$ integrin function. Localization of stimulatory epitopes. *J. Biol. Chem.* **271**, 3046–3051
 48. Cho, J. Y., Fox, D. A., Horejsi, V., Sagawa, K., Skubitz, K. M., Katz, D. R., and Chain, B. (2001) The functional interactions between CD98, $\beta 1$ -integrins, and CD147 in the induction of U937 homotypic aggregation. *Blood* **98**, 374–382
 49. Van Aghthoven, J. F., Xiong, J. P., Alonso, J. L., Rui, X., Adair, B. D., Goodman, S. L., and Arnaout, M. A. (2014) Structural basis for pure antagonism of integrin $\alpha V\beta 3$ by a high-affinity form of fibronectin. *Nat. Struct. Mol. Biol.* **21**, 383–388
 50. Copié, V., Tomita, Y., Akiyama, S. K., Aota, S., Yamada, K. M., Venable, R. M., Pastor, R. W., Krueger, S., and Torchia, D. A. (1998) Solution structure and dynamics of linked cell attachment modules of mouse fibronectin containing the RGD and synergy regions: comparison with the human fibronectin crystal structure. *J. Mol. Biol.* **277**, 663–682
 51. Beglova, N., Blacklow, S. C., Takagi, J., and Springer, T. A. (2002) Cysteine-rich module structure reveals a fulcrum for integrin rearrangement upon activation. *Nat. Struct. Biol.* **9**, 282–287
 52. Zhang, P., Fu, C., Hu, Y., Dong, C., Song, Y., and Song, E. (2015) C6-ceramide nanoliposome suppresses tumor metastasis by eliciting PI3K and PKC ζ tumor-suppressive activities and regulating integrin affinity modulation. *Sci. Rep.* **5**, 9275
 53. Pike, K. A., Kulkarni, S., and Pawson, T. (2011) Immature T-cell clustering and efficient differentiation require the polarity protein Scribble. *Proc. Natl. Acad. Sci. U.S.A.* **108**, 1116–1121
 54. Mould, A. P., Symonds, E. J., Buckley, P. A., Grossmann, J. G., McEwan, P. A., Barton, S. J., Askari, J. A., Craig, S. E., Bella, J., and Humphries, M. J. (2003) Structure of an integrin-ligand complex deduced from solution x-ray scattering and site-directed mutagenesis. *J. Biol. Chem.* **278**, 39993–39999
 55. Takagi, J., Strokovich, K., Springer, T. A., and Walz, T. (2003) Structure of integrin $\alpha 5\beta 1$ in complex with fibronectin. *EMBO J.* **22**, 4607–4615
 56. Crump, J. G., Swartz, M. E., and Kimmel, C. B. (2004) An integrin-dependent role of pouch endoderm in hyoid cartilage development. *PLoS Biol.* **2**, E244
 57. Orlando, R. A., and Cheresch, D. A. (1991) Arginine-glycine-aspartic acid binding leading to molecular stabilization between integrin $\alpha V\beta 3$ and its ligand. *J. Biol. Chem.* **266**, 19543–19550
 58. Müller, B., Zerwes, H. G., Tangemann, K., Peter, J., and Engel, J. (1993) Two-step binding mechanism of fibrinogen to $\alpha IIb\beta 3$ integrin reconstituted into planar lipid bilayers. *J. Biol. Chem.* **268**, 6800–6808
 59. Peerschke, E. I. (1999) Maintenance of GPIIb–IIIa avidity supporting “irreversible” fibrinogen binding is energy-dependent. *J. Lab. Clin. Med.* **134**, 398–404
 60. Kasirer-Friede, A., Kang, J., Kahner, B., Ye, F., Ginsberg, M. H., and Shattil, S. J. (2014) ADAP interactions with talin and kindlin promote platelet integrin $\alpha IIb\beta 3$ activation and stable fibrinogen binding. *Blood* **123**, 3156–3165
 61. Dickreuter, E., Eke, I., Krause, M., Borgmann, K., van Vugt, M. A., and Cordes, N. (2016) Targeting of $\beta 1$ integrins impairs DNA repair for radiosensitization of head and neck cancer cells. *Oncogene* **35**, 1353–1362
 62. Kimura, H., Tome, Y., Momiyama, M., Hayashi, K., Tsuchiya, H., Bouvet, M., and Hoffman, R. M. (2012) Imaging the inhibition by anti- $\beta 1$ integrin antibody of lung seeding of single osteosarcoma cells in live mice. *Int. J. Cancer* **131**, 2027–2033
 63. Park, C. C., Zhang, H. J., Yao, E. S., Park, C. J., and Bissell, M. J. (2008) $\beta 1$ integrin inhibition dramatically enhances radiotherapy efficacy in human breast cancer xenografts. *Cancer Res.* **68**, 4398–4405
 64. Mould, A. P., Garratt, A. N., Puzon-McLaughlin, W., Takada, Y., and Humphries, M. J. (1998) Regulation of integrin function: evidence that bivalent-cation-induced conformational changes lead to the unmasking of ligand-binding sites within integrin $\alpha 5\beta 1$. *Biochem. J.* **331**, 821–828
 65. Parsons, M., Messent, A. J., Humphries, J. D., Deakin, N. O., and Humphries, M. J. (2008) Quantification of integrin receptor agonism by fluorescence lifetime imaging. *J. Cell Sci.* **121**, 265–271
 66. Collins, T. J. (2007) ImageJ for microscopy. *BioTechniques* **43**, S25–S30
 67. O’Boyle, N. M., Banck, M., James, C. A., Morley, C., Vandermeersch, T., and Hutchison, G. R. (2011) Open Babel: An open chemical toolbox. *J. Cheminform.* **3**, 33
 68. Mould, A. P., Burrows, L., and Humphries, M. J. (1998) Identification of amino acid residues that form part of the ligand-binding pocket of integrin $\alpha 5\beta 1$. *J. Biol. Chem.* **273**, 25664–25672
 69. Humphries, J. D., Askari, J. A., Zhang, X. P., Takada, Y., Humphries, M. J., and Mould, A. P. (2000) Molecular basis of ligand recognition by integrin $\alpha 5\beta 1$. II. Specificity of Arg-Gly-Asp binding is determined by Trp157 of the α subunit. *J. Biol. Chem.* **275**, 20337–20345
 70. Askari, J. A., Tynan, C. J., Webb, S. E., Martin-Fernandez, M. L., Balles-trem, C., and Humphries, M. J. (2010) Focal adhesions are sites of integrin extension. *J. Cell Biol.* **188**, 891–903
 71. Askari, J. A. (2006) *Conformational Changes in Integrin $\alpha 5\beta 1$* . Ph.D. thesis, University of Manchester, UK
 72. Ni, H., and Wilkins, J. A. (1998) Localisation of a novel adhesion blocking epitope on the human $\beta 1$ integrin chain. *Cell Adhes. Commun.* **5**, 257–271